"DEVELOPMENT OF LITHIUM TITANATE CERAMIC FOR THE TEST BLANKET MODULE (TBM) IN FUSION REACTOR"

A Thesis Submitted in Partial Fulfillment of the

Requirements for the Degree of

Master of Technology (Research)

in

ENGINEERING

by

Bhabani Sankar Sahu
(Roll No: 608CR301)

Supervisor:

Dr. Ranabrata Mazumder

DEPARTMENT OF CERAMIC ENGINEERING

NATIONAL INSTITUTE OF TECHNOLOGY ROURKELA

November, 2010

NATIONAL INSTITUTE OF TECHNOLOGY

Rourkela, INDIA

CERTIFICATE

This is to certify that the thesis entitled **"DEVELOPMENT OF LITHIUM TITANATE CERAMIC FOR THE TEST BLANKET MODULE (TBM) IN FUSION REACTOR" being** submitted by **Mr. Bhabani Sankar Sahu**, for the degree of **Master of** Technology (Research) **in Ceramic Engineering** to the National Institute of Technology, Rourkela, is a record of bonafide research work carried out by him under my supervision and guidance. His thesis, in my opinion, is worthy of consideration for the award of degree of Master of Technology (Research) in accordance with the regulations of the institute.

The results embodied in this thesis have not been submitted to any other university or institute for the award of a Degree.

Supervisor

Prof. R Mazumder

Department of Ceramic Engineering
National Institute of Technology
Rourkela

CONTENTS

Chapter IV - Experimental Work

Chapter V - Results and Discussions

Abstract

Lithium-based ceramic, Li_2TiO_3, is being considered as promising solid breeder materials in the tritium breeding blanket of thermonuclear fusion reactors, because of its reasonable lithium atom density, prominent tritium release rate at low temperatures between 200 and 400^oC, its low activation characteristics, low thermal expansion coefficient, high thermal conductivity. For tritium recovery purpose samples having 85-90% of true density with open porosity (around 5%) is required. Uniform small grain size distribution (having diameter between 2-4μm) is preferable as activation energy for tritium diffusion through grain is higher compared to grain boundary. Solid state method requires higher calcination temperature, producing coarser particle and impurity, which adversely affects in achieving high sintered density (above 85% of theoretical density) and forms large grain size with entrapped closed pore inside the grain.

In the current work Li_2TiO_3 powder was synthesized by solution combustion technique using cheaper precursor of titanium i.e. TiO_2. We found that by controlling the citrate to metal ratio and pH of the solution, phase purity can be achieved in as burnt powder. We observed that phase purity and powder morphology depends on the citrate to metal ratio and pH of the solution. The particle size of Li_2TiO_3 powder (prepared at C/M=1 and pH=1) was found to be 100-200 nm and surface area was 62 m^2/g. It was found that Li_2TiO_3 powder can be sintered at a temperature as low as 900^oC with a density more than 90% of the theoretical density. The thermal expansion behavior was investigated by thermo dilatometery of sintered specimens in air atmosphere. Thermal diffusivity measured by laser flash method. Thermal conductivity value depends on the density of the sample. AC impedance method has been used to characterize electrical property of the sintered sample as tritium diffusion is related to the Li^+ ion conductivity in Li_2TiO_3. Impedance data, measured on sample of small grained Li_2TiO_3ceramics, showed differences for different sintering temperature in air which is doubtless an effect of the variation in microstructure. Neutron activation studies have been done on Li_2TiO_3 powder to find out whether impurity content in the breeder material absorbing the neutrons and forming any long lived activation product.

Acknowledgements

I wish to express my most sincere heartfelt gratitude to Prof. R. Mazumder, Department of ceramic Engineering, N.I.T Rourkela for his suggestion and guidance during the entire research work. I express my sincere thanks to Prof. S. Bhattacharyya, for his cooperation and suggestions for betterment.

I express my sincere thanks to Prof J. Bera, Head, Ceramic Engineering for providing me all the departmental facilities required for the completion of the thesis.

I am grateful to Prof. S.K. Pratihar, who's out of the way help and guidance helped me during the research work. I am also thankful to all other faculty members of Ceramic Engineering Department, NIT Rourkela for their invaluable advice, constant help, encouragement, inspiration and blessings.

I am grateful to Mr. Paritosh Chaudhuri, Scientist(E), Institute of Plasma Research (IPR), Gandhinagar for providing me Neutron Irradiation tests and other characterization facilities for completing the work. The author also gratefully acknowledges the research internship provided by IPR, Gandhinagar and also to BRFST (Board of Research in Fusion Science and Technology) for providing junior research fellowship.

Submitting this thesis would have been a Herculean job, without the constant help, encouragement, support and suggestions from my friends and seniors, especially Ganesh bhai, Abhisek and all the research scholars of Ceramic Engineering Department, NIT Rourkela.

Last but not the least, I would like to thank my parents, younger brother for their support for choices in all my life and their love, which has been a constant source of strength for everything I do. My special thanks go to Arpita, Amiya and Pramod who are always with me in the all difficult situation.

(Bhabani Sankar Sahu)

LIST OF FIGURES

LIST OF TABLES

Chapter I

Introduction

1.1 Introduction:

To meet worlds primary energy needs each year, the world consumes energy roughly equivalent to 3 million tonnes of coal. Of this, three-quarters comes from fossil fuels, all of which when combusted release carbon dioxide (CO_2); while around 6% is supplied by the very low CO_2-emitting technology of nuclear power. All nuclear power stations in operation today rely on fission – the splitting of large atomic nuclei, in particular the very heavy elements like uranium and plutonium [1]. Most nuclear power stations are fuelled by uranium. An alternative approach to have usable energy production depends on nuclear fusion. The basis of this is the release of energy when very light nuclei are brought together to form more stable heavier ones. Fusion research holds out the promise of providing a clean, sustainable energy supply to contribute to the increasing needs of our civilization. Nuclear fusion is the process that powers the sun and other stars. Research into nuclear fusion to generate electricity is ongoing despite of huge technical challenges.

1.2 Background of Fusion:

Nuclear reactions are different from chemical reactions in that they involve the protons and neutrons in the nucleus, rather than electrons. Like chemical reactions, nuclear reactions can involve either a net absorption or a net release of energy. To achieve a release of energy in a fusion reaction, smaller, less stable nuclei must be joined together to form a more stable nucleus. The energy associated with binding, the initial components is greater than that associated with the reaction products, and it is this energy difference that is released during fusion. Interestingly, these small differences in binding energy are reflected in the observable masses of the various reaction components; via Albert Einstein's famous equation describing the equivalence of mass and energy: $E = mc^2$. This states that energy = mass × (speed of light)^2. That is, the components after the reaction actually weigh less than those before the reaction and the mass difference is released as energy [2]. Einstein's equation gives an indication of the scale of the proportionality between mass and energy, and it explains why very small changes of mass in nuclear fuel can release a great deal of usable energy.

Binding Energy:

The neutrons and protons are kept stable in every atom's nucleus by attractive nuclear force which is of the order of 10^{-15}m. The relative stabilities of the nuclei of different elements are determined by their binding energies, that is, how much energy is required to remove a proton or neutron from the nucleus. If the binding energy of each nucleus is plotted as a function of

the number of protons and neutrons it contains, a curve of binding energy is obtained. As seen in the (Fig.1.1), nuclei with a small number of neutrons and protons have a low binding energy.

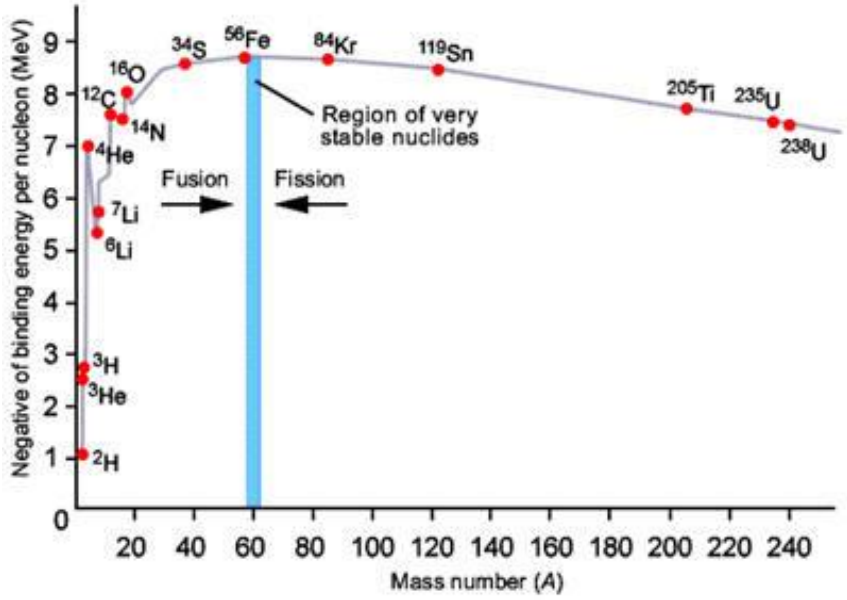

Fig.1.1 Variation of Binding energy with Mass number of elements

Such nuclei are easier to break apart and are not as stable as nuclei with larger numbers of protons and neutrons. If these nuclei are fused, it was found that the total binding energy of the product nuclei to be less than the reacting nuclei; so the loss of this energy will be known as fusion energy. As the number of neutrons and protons increases, the binding energy reaches a peak and then drops off again. Nuclei at the peak are the most tightly bound and correspond to elements near iron in the periodic table. As neutrons and protons continue to be added, the nucleus becomes less tightly bound. It is due to the fact that the size of the nucleus increases as the number of nucleons added and consequently the electrostatic force dominates over the short range nuclear force which ranges in the order of femtometer. In uranium and plutonium nuclei, at the far right end of the plot, break into smaller nuclei, the newer elements are harder to break apart. Elements on the far left of the binding energy curve release energy by fusion, while elements on the far right release energy via fission. The energy released arises from the difference between the nuclear binding energies of the initial and final components.

Fusion Reactions:

Fusion is a potential energy source with a major advantage of having an almost unlimited fuel supply. The next generation fusion reactors will be based on the deuterium-tritium (D&T) reaction (Fig.1.2) since it is the easiest fusion reaction to achieve [3]. The reacting nuclei must collide hard and often to undergo fusion. The requirements of multiple, high-energy collisions

of fuel nuclei are met in a hot, dense plasma. This is the reaction between the heavy isotopes of hydrogen, deuterium (D), and tritium (T) which on fusion yields an alpha particle (‘He) and a neutron and 17.6MeV of energy,viz [4].

$$D + T \rightarrow He_2^4 + n + 17.6Mev \qquad (1.1)$$

The released energy is taken up by the two new particles in inverse proportion to their masses. That is, one fifth is taken up by the kinetic energy of the helium nucleus and four-fifths by the kinetic energy of the neutron. As an electrically neutral particle, the neutron is unaffected by any magnetic fields. These fast neutrons are emitted in all directions and are the primary means by which energy leaves the fusion reactor. Many of these neutrons would leave the reactor on its outer edge and come to rest in a component known as “the blanket”. This contains material designed to slow down the fast neutrons and in doing so become heated. This heat is, in turn transferred to a medium such as high-pressure helium or steam. This hot, high-pressure gas can be used to drive an electricity-generating turbine. Some modules of the power-station blanket would include lithium, which reacts with the fast neutrons to generate tritium, one of the two fuels required for the reaction. In this way a fusion power station could produce one component of its own fuel in situ.

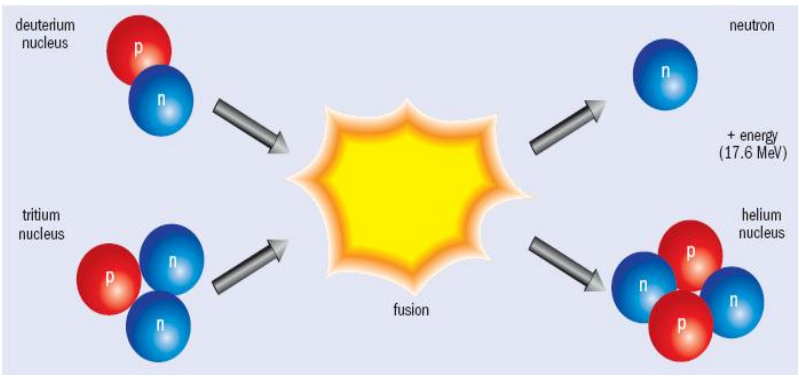

Fig. 1.2 The fusion reaction of deuterium and tritium.

Operation of a power plant with the (DT) fuel cycle requires introduction of an essentially continuous supply of deuterium and tritium into the reactor chamber. Deuterium is readily available as heavy water (D_2O) from which deuterium can be separated by simple electrolysis. Since the earth’s waters contain about 10^{13} metric tons (t) of deuterium, there is an essentially unlimited supply of deuterium available for all nations.

But naturally occurring tritium is in-sufficient in quantity and concentration for use as a fuel. It is only 10^{-16}% of total Hydrogen found on earth. However, tritium can be produced from lithium by the following nuclear reactions:

$$^{6}_{3}Li + n \rightarrow T + ^{4}_{2}He + 4.8Mev \quad (1.2)$$

$$^{7}_{3}Li + n \rightarrow T + n + ^{4}_{2}He + 2.5Mev \quad (1.3)$$

1.3 Why lithium is required for tritium breeding?

Lithium has been identified as the only viable element to breed tritium. Naturally occurring lithium is composed of two stable isotopes, ^{6}Li and ^{7}Li, the latter being the more abundant (92.5% natural abundance). Both natural isotopes have anomalously low nuclear binding energy per nucleon compared to the next lighter and heavier elements, helium and beryllium, which means that alone among stable light elements. For atoms with low atomic numbers, a nucleus that has a different number of protons than neutrons can potentially drop to a lower energy state through a radioactive decay that causes the number of protons and neutrons to more closely match. The neutron and the proton are different types of fermions. The Pauli Exclusion Principle is a quantum mechanical effect that prohibits identical fermions, such as multiple protons, from occupying the same quantum physical state at the same time. Thus every proton in the nucleus must occupy a different state, with its own energy level, and the same rule applies to all of the neutrons. This prohibition does not apply to a proton and neutron occupying the same quantum state. Since lithium ^{7}Li has an extra neutron in its atomic nuclei and thus had a lower value of proton to neutron ratio which makes its binding energy to be low. This makes Lithium to be suitable for tritium breeding than any other element.

1.4 Lithium bearing ceramics for Tritium production:

Interest in the use of solid lithium-based materials as tritium breeders for fusion blankets has grown since the late 1970s. Ceramic lithium compounds are used as breeder for fusion blanket because of more favorable physical characteristics for the severe operating conditions of high temperatures and intense neutron fluxes. Lithium-containing ceramics such as Li_2O, γ-$LiAlO_2$, Li_4SiO_4, Li_2ZrO_3 and Li_2TiO_3 have been considered as candidates for tritium breeding materials in D–T fusion reactors of the ITER test blanket module (TBM) for DEMO reactor [5-10]. The tritium breeder blanket in the fusion reactor serves two primary functions: breeding tritium and converting the released energy into sensible heat, both of which are critical to fusion power development. Principal requirements to be fulfilled by the breeder material are to 1) breed and release tritium, 2) possess physical and chemical stability at high temperature, 3)

display compatibility with other blanket components, and 4) exhibit adequate irradiation behavior. Because of their overall desirable properties, lithium-containing ceramics are recognized as attractive tritium breeding materials for fusion reactor blankets.

1.5 Function of the tritium breeder in Test blanket Module (TBM):

DEMO and ITER:

DEMO is the demonstration reactor which is going to be constructed and tested before the actual realization of ITER (International thermonuclear experimental reactor) that can produce electrical power. To achieve this in the shortest timescale, studies have shown that aside from the operation of ITER, a parallel programme of materials testing would be needed. In particular DEMO will rely on a "hot breeding blanket" to convert the kinetic energy of the neutrons created in the plasma chamber into heat [17].

A test blanket module relies on the use of lithium ceramics as breeder material, beryllium as neutron multiplier, helium as coolant, and martensitic steel as structural material. The lithium breeder is impounded in the structural material to form the blanket. The blanket differs essentially by the architecture of their cooling system. Two kinds of configuration has been accepted, one is of the "Breeder Inside Tube" (BIT) type (that is the breeder material is in form of pellets stacked inside tubes, with the helium coolant flowing outside the tubes) while the other one is of the "Breeder Outside Tube" (BOT) type (the coolant flows in tubes, with the breeder material in form of pebbles located outside).

Indeed the production of one tritium atom by the 6Li(n, α)T reaction consumes one neutron, while its fusion with a deuterium generates only one neutron which exhibits a significant probability (30-35%) of not being available for tritium production (because of parasitic absorbtions in blanket structures, of streaming through the blanket opening). These neutron losses must therefore be compensated. Hence a neutron multiplier is incorporated in the blanket, in addition to a 6Li-rich compound, like beryllium or lead.

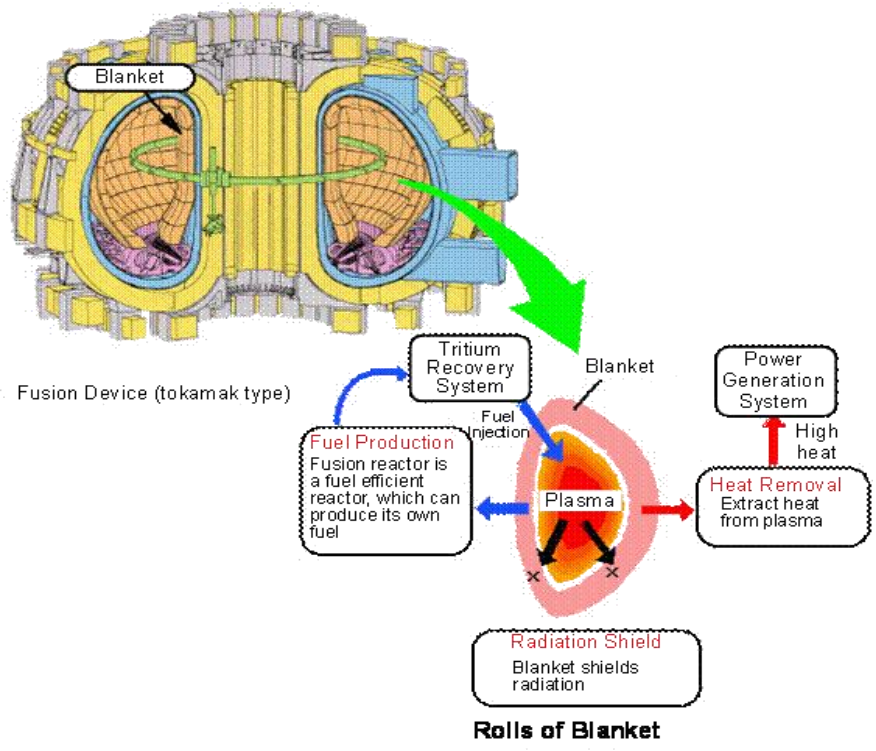

Fig. 1.3 Schematic diagram of TBM

TBM has two crucial functions (Fig. 1.3). It produce and recover all tritium produce from the DT reaction and secondly to act as a heat exchanger i.e to extract the heat from plasma and supplies it to the power generation system.

1.6 Different kinds of breeder materials and their properties:

Lithium-based ceramics such as Li_2O, γ-$LiAlO_2$, Li_4SiO_4, Li_2ZrO_3 and Li_2TiO_3 have been considered as candidates for tritium breeding materials in D–T fusion reactors of the ITER test blanket module (TBM) for DEMO reactor [5-9, 11-16].

Lithium oxide Li_2O:

- Lithium oxide (Li_2O) is an attractive ceramic breeder material because of its high lithium atom density for tritium breeding, high thermal conductivity, good tritium release properties and low activation.
- However, at temperatures below a moisture-pressure-dependent critical value (e.g., 366°C at 10 Pa), LiOH will precipitate out as a separate phase, thereby increasing tritium retention to unacceptable levels.
- This also results in transport of Lithium to cooler zones of Blanket.

- At high temperatures (e.g., 800-1000°C), transport of vapor phase LiOH, as well as chemical incompatibility with structural materials, may cause design problems.
- Thus, controlling moisture pressure is essential to Li_2O performance.
- Tritium breeding is marginal without a neutron multiplier.
- Acceptable tritium recovery is a key feasibility issue.

Lithium aluminate Li_2AlO_3:

- Lithium aluminate might be superior to Li_2O because of its higher melting temperature and better swelling resistance, broader operating temperature excellent irradiation behavior.
- However it requires a higher minimum operating temperature to maintain low tritium inventory.
- Effective neutron multiplier required for adequate breeding.
- Tritium release characteristics are poor.

Lithium zirconate (Li_2ZrO_3) :

- Lithium zirconate (Li_2ZrO_3), while not as attractive as Li_2O with regard to breeding, heat transport and activation.
- Activation of zirconium is a concern, though it is small in comparison to that from the blanket structural materials.
- It also exhibits low tritium retention at low operating temperatures, compatibility and stability (chemical, irradiation, and microstructural) is at least as good as the other ternaries (Li_4SiO_4 and $LiAlO_3$) and much better than that of Li_2O.
- Li_2ZrO_3 has long-term radioactive characteristics than Li_2O, Li_4SiO_4**,** Li_2TiO_3

Lithium silicate (Li_4SiO_4):

- Lithium ortho-silicate (Li_4SiO_4) possesses good lithium atom density and exhibits the most favorable tritium release behavior
- Li_4SiO_4 does not produce long-lived activation products during the irradiation process
- Material fragment severely, due to differential thermal expansion
- Highest lithium vaporization rate and little sensitivity to moisture.

Lithium Titanate (Li_2TiO_3):

Low-activation ceramic material for use in tritium breeding and have good tritium release properties [13-16]

- Better thermal conductivity than other breeder materials as well high thermal stability
- High chemical stability, high mechanical resistance
- Reactivity to moisture is very lees compared to other breeder ceramics
- Good compatibility with structural materials

References:

1. Benn T., 1996 The Benn Diaries (Arrow Books).
2. Arthur Beiser 6th Edition ,Tata McGraw-Hill Edition
3. Hartley J. N., B. F. Gore and J. R. Young, Energy Vol. 3. (1978) P. 337-346
4. Bosch H.S et al. 1996 Fusion 38 415–449.
5. Johnson C.E., Hollenberg G.W., Roux N., Watanabe H., Fusion Eng. Des. 8, (1989), 145
6. Roux N., Avon J., Floreancig A., Mougin J., Rasneur B., Ravel S., J. Nucl. Mater. 233-237 (1996) 1431 - 1435
7. Lulewicz J.D., Roux N., Fusion Eng. Des. 39–40, (1998), 745–750
8. Wu X., Wen Z., Xu X., Gu Z., Xu X., J. Nucl. Mater. 373, (2008), 206–211
9. Johnson C.E., Ceramics International 17, (1991), 253-258
10. Johnson C.E., J. Nucl. Mater. 270, (1999), 212-220
11. Lidsky L.M., Nuclear Fusion, 15, (1975), 151-173
12. Roux N., Tanaka S., Johnson C.E., Verrall R., Fusion Eng. Des. 41, (1998), 31–38
13. Roux N., Hollenberg G., Johnson C., Noda K., Verrall R., Fusion Eng. Des.27, (1995), 154-166
14. Gierszewski P., Fusion Eng. Des. 39–40 (1998) 739–743
15. Miller J.M., Hamilton H.B., Sullivan J.D., J. Nucl.Mater. 212–215 (1994) 877
16. Kopasz J.P., Miller J.M., Johnson C.E., J. Nucl. Mater. 212 (1994) 927
17. Proust E., Anzidei L., Casini G., Donne M.D., Giancarli L.and Malang S.,Fusion Eng. Des. 22 (1993) 19-33

Chapter II

Literature Review

2.1 Phase diagram and crystal structure of Li_2TiO_3:

Kleykamp et al. [1,2] studied the phase equilibria of the pseudo-binary Li_2O-TiO_2 system and the stoichiometry shift of Li_2TiO_3 during the Li transmutation. The binary Li_2O-TiO_2 system is characterized by four ternary oxides: Li_4TiO_4, Li_2TiO_3, $Li_4Ti_5O_{12}$, and` the high-temperature phase $Li_2Ti_3O_7$ which decomposes eutectoidally at about 950°C. The Li_2TiO_3 exists in three modifications, α, β and γ [3,4]. The α–phase of Li_2TiO_3 is metastable and has a monotropic transformation to β -Li_2TiO_3 by heating above 300°C.

The low-temperature β -phase is monoclinic, and crystallizes in the Li_2SnO_3-type structure with the space group C2/c (No. 15), Z=8, and the lattice parameters a=504.1 pm, b =880.6 pm, c =972.7 pm and β =100.08.

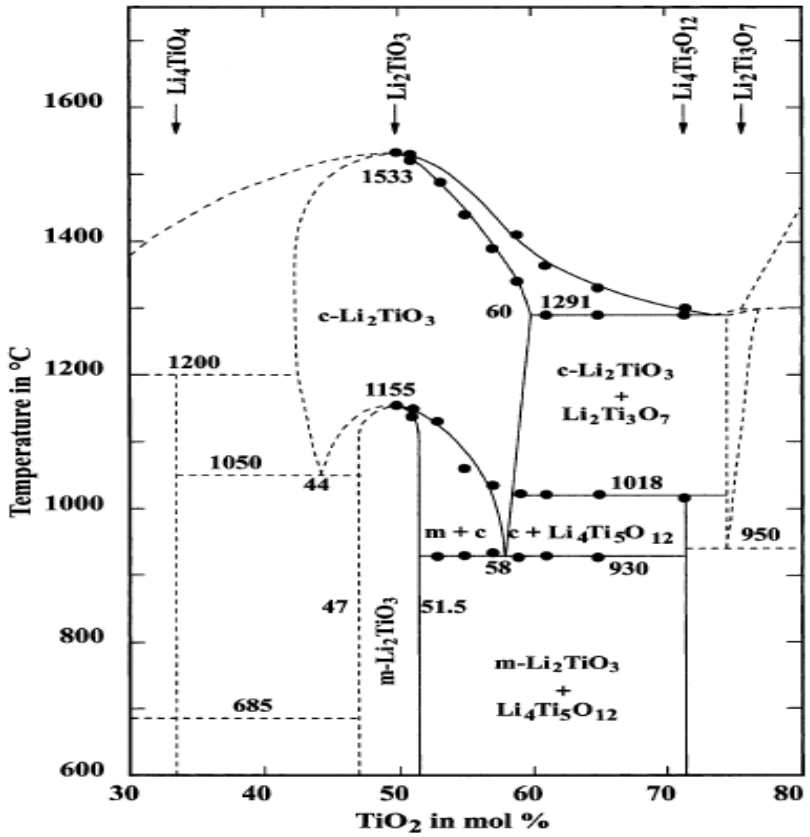

Fig. 2.1 Phase diagram of Li_2TiO_3

The β-modification of Li_2TiO_3 has a narrow homogeneity range between 47 and 51 mol% TiO_2 and 52 mol% TiO_2 (Fig. 2.1). The room temperature (RT) X-ray density of Li_2TiO_3 is ρ=3.43 g/cm^3. The β to γ (monoclinic to /cubic) transformation of stoichiometric Li2TiO3 is reported at 1155°C. The γ -Li_2TiO_3 has high temperature cubic phase and crystallizes in the NaCl-type

structure, Z=4/3, with the RT lattice parameter a=415.05 pm. The RT X-ray density is ρ=3.40 mg/m^3 [5] respectively. Li_2TiO_3 undergoes an order-disorder phase transition at 1215°C. The temperature of the order-disorder transition decreases to either side of the Li_2TiO_3 composition. The spinel phase $Li_4Ti_5O_{12}$, has an upper limit of stability at 1015±5°C, above which it decomposes to high temperature phase Li_2TiO_3 and $Li_2Ti_3O_7$. $Li_2Ti_3O_7$ has a lower limit of stability at 957±20°C, below which it decomposes to $Li_4Ti_5O_{12}$ and rutile [6].

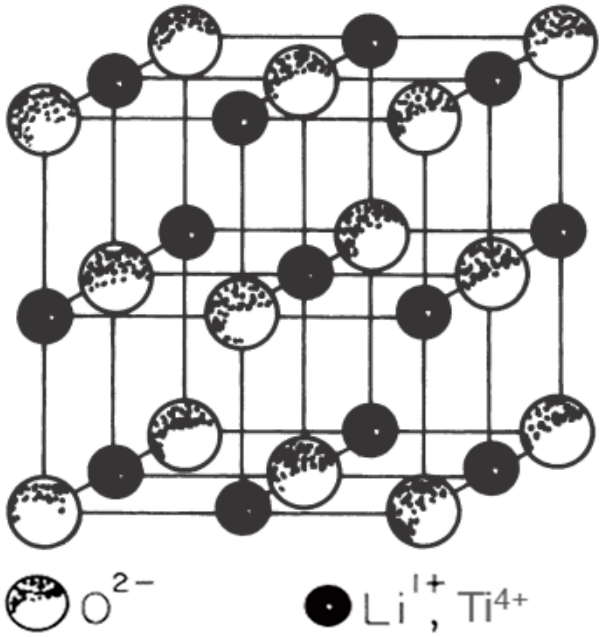

Fig. 2.2 Crystal structure of Li_2TiO_3

Lang et al. [7] has described Li_2TiO_3 as iso-structural with Li_2SnO_3, a derivative structure of sodium chloride. The reorientation in the unit cell of the NaCl structure gives rise to the monoclinic structure of Li_2TiO_3. The cations i.e Li and Ti are randomly distributed in the cation sites of rocksalt structure. It is proposed that in Li_2TiO_3 two types of layer structure exist (as it is iso-structural with Li_2SnO_3)[8]; one composed of Lithium occupied octahedra and the other composed of Lithium and Titanium occupied octahedra in 1:2 ratio stacked alternately perpendicular the ab plane. In Li_2TiO_3 all the octahedral edges are shared between two Ti, two Li, or one Ti and one Li. The mean O-O distances for the three categories takes different values showing the cation repulsion is chiefly responsible for the distortion in the rocksalt structure [6,7]

2.2 Synthesis and sintering of Li_2TiO_3 Breeder Materials:

Lithium titanate (Li_2TiO_3) was synthesized through different techniques by various researchers. The selected techniques for synthesizing Lithium titanate depend on cost as well as applications. The quality of the final powders is not only influenced by the synthesis route but also by the starting precursors used. Size of the particle determines the properties of final material.

Li_2TiO_3 has been prepared by basically two techniques (1) Solid state reaction based (2) Chemical solution based technique. Solid state reaction based techniques involves the mixing of precursors in their oxide or carbonate form, either by hand mixing or by high energy ball milling; whereas chemical methods involves sol-gel processing, hydrothermal process, co-precipitation technique, soft solution processing and combustion synthesis.

2.2.1 Conventional Solid state technique:

Roux et al. [9] synthesized lithium titanate by solid state reaction technique by taking the precursors Li_2CO_3 and TiO_2 which requires a temperature of 850^oC/3hrs to get the final powder. They have achieved only 82% of true density at 1050^oC. Critical issues, namely, materials fabricability, compatibility, themlomechanical, irradiation and tritium release behaviours are addressed. Results of investigations show that this ceramic as promising materials for the ITER breeding blanket.

Wu et al. [10] prepared the samples by solid state synthesis route taking Li_2CO_3 and TiO_2 . Appropriate amounts of Li_2CO_3 (A.R.) and TiO_2 (A.R.) powders corresponding to the Li/Ti=2 and the final ceramic products were blended by planetary ball milling for 4 h with ethyl alcohol as the milling medium.Li_2TiO_3 powders were formed by calcining the dried precursors at 700^0C for 4 h in air atmosphere. The resulted powder was used for the making of pebbles by wet chemistry method. The powder were compacted and sintered at 1050^oC/3hrs.

2.2.2 Synthesis of Li_2TiO_3 by solution route:

The advantage of chemical processing lies on the basis of homogenous mixing of precursors in atomic and molecular level and the ease of getting phase pure material at low temperature; it also ensure the synthesis of the crystallized powder with submicron particles. The properties of the powder depend on different preparation methods.

Li_2TiO_3 by Sol-gel technique:

X. Wu et al. [11] studied the water based sol-gel method for the preparation of Li_2TiO_3. In this work they had used de-ionized water instead of ethanol as the reaction medium in conventional hydroxide–alkoxide sol–gel route. In this process $LiNO_3$ and $Ti(C_6H_6O_7)_2$ was used as the lithium source and titanium source, respectively. Citric acid ($C_6H_8O_7$) was used as the chelating agent and ammonia solution ($NH_3.H_2O$) was used to adjust the pH of the solution. The precursor chemicals are mixed and heated at 60^oC to get the gel and was dried at 150^oC/12hr. Calcination of the dried gel performed at 500^oC/4hr. The primary particle size of the powder was smaller than 50 nm confirmed by TEM. The sintered pellets fabricated from the powder at 1100°C for 4 h reached a density of 90% of T.D. But the microstructure shows presence of significant amount of closed pore which may be detrimental for tritium release.

Mohammadi et al. [12] have been successfully prepared nano-structured and mesoporous lithium titanate thin films and powders via a particulate sol–gel route at low temperature. Titanium isopropoxide and lithium nitrate were used as titanium and lithium precursors, whereas Hydroxypropyl cellulose (HPC) was used as a polymeric fugitive agent. Based on XRD analysis, the average crystallite size of the powders was calculated less than 5 nm at 400^oC.

Polymer solution technique:

Researcher was used polymer solution technique for synthesis of inorganic oxide powder using PVA (polyvinyl alcohol), PEG (polyethylene glycol) or EG ($HOCH_2CH_2OH$, ethylene glycol) as a polymer carrier which is used to make the soft-solution processing easier and to yield nano size powder. The polymer ensures a homogeneous distribution of the metal ions in its polymeric network structure and hinders their segregation or precipitation from the solution. In the solution involving a polymer and nitrate ions, a continuous long chain polymer prevents a linkage between the cations and it limits their agglomeration and precipitation [13-15]. Jung et al. [16] used polymer solution route to prepare Li_2TiO_3 powder by using titanium(IV) isopropoxide [$Ti(OC_3H_7)_4$], lithium nitrate ($LiNO_3$) and ethylene glycol(EG) as precursor material. Metal to EG ratio was around 1:4. The powders obtained were porous and the particle size was around 70nm. Similar 90% density can be achieved when sintered 1100^oC/ 2hrs.

Hoshino et al. [17] followed sol-gel technique to synthesize Li_2TiO_3. The precursors used were costly Lithium alkoxide (LiO-i-C_3H_7 or LiO-C_2H_5), Titanium isopropoxide ($Ti(OC_3H_7)_4$) and

the reaction medium was C_2H_5OH. The effect of excess Li_2O has also been studied; the crystal structure and the non-stoichiometry of the Li_2O added Li_2TiO_3 have been extensively investigated by means of XRD and thermogravimetry.

Solution combustion synthesis:

Recently, combustion synthesis has been shown to be a useful preparative route for multi-component oxide powders. Typically, the products of combustion synthesis are highly reactive, contain minimum levels of impurities, can be prepared rapidly and normally do not require specialized equipment for their preparation. Precursors are often prepared from an aqueous solution of the metal nitrates and an organic complexant such as, carboxylate azides [18], citric acid [19], urea [20] or glycine [21]. An important advantage of such precursors is that the cation stoichiometry can be controlled precisely through complexometric titration of the metal nitrate stock solutions [22].

Jung et al. [23-25] reported synthesis of Li_2TiO_3 by Glycine-nitrate auto-combustion technique where the source of Ti was Ti-nitrate solution, which was prepared by hydrolysing $TiCl_4$ followed by dissolving precipitate of Ti-hydroxide in HNO_3. They also studied the effect of other fuel such as citric acid and urea on the phase formation. The surface area of the synthesized powder was in the range of 10 to 14 m^2/gm and the primary particle size is found to be about 30 nm.They showed that combustion synthesized Li_2TiO_3 powders can be sintered to 82% of TD at 1000^{o}C for 4 hrs and 85% of TD at 1100^{o}C for 4 hrs. Latter they have developed the pebbles of Li_2TiO_3 by dry rolling granulation process (DRGP).

Sinha et al. [26] reported single step solid-liquid combustion synthesis of Li_2TiO_3 starting from hydrated titania and $LiNO_3$. But the complete dissolution of hydrated titania in aqueous solution was difficult and it yields inhomogenity in solution mixture resulted in unwanted phases in the powder which is clearly reflected in the XRD pattern. However the synthesized powder requires ball milling to get a density 90% of TD at 1150^{o}C. But fractured surface of sintered specimen shows huge entrapped pore inside the grain.

Rhee et al. [27] studied the densification of Li_2TiO_3 by rapid sintering technique. The density of the rapidly sintered Li_2TiO_3 pellet remarkably increased up to 89% of TD than conventional sintering process. The schedule for rapid sintering followed is, the samples were rapidly heated

at the rate of 10^{o}C /min to 1300^{o}C and then annealed at 1000^{o}C for 1h. But still it is not effective to keep the grain size below 5μm.

Deganello et al. [19] used citrate–nitrate auto-combustion for synthesis of perovskite-type nano powders. They varied the pH of the solution and found that low pH are generally deleterious for the phase composition and/or for the morphology of the final product and high pH values may cause dopant segregation and high agglomeration. The idea behind varying the pH is to have a homogenous solution of metal with the complexing agent to form a stable complex, which further facilitates the combustion reaction. Complete complex formation means binding all the metal cations by the chelating ligands. Complexing potential of citric acid strongly depends upon its dissociation. At low pH value it poorly dissociates, hence does not form complete metal complex and as well no more citric acid is left for the citrate–nitrate auto-combustion reaction. The citric acid/metal nitrates should be carefully selected in order to avoid precipitation of the most insoluble compounds or segregation of the dopant. Moreover, high C/M values increase the formation temperature of the perovskite-type structure.

However, to best of our knowledge, there are no reports available on the effect of pH variation and citrate to metal ratio in solution combustion synthesis of Li_2TiO_3.

2.3 Thermal properties of Li_2TiO_3:

Thermal conductivity is a material property and of major importance for materials that act as heat transfer agents. Generally, thermal conductivity decreases with increasing porosity and increasing temperature and is very sensitive to impurities and defects coming from the material processing. The effective thermal conductivity depends on the size and density of pallets, surface conditions, packing fraction, gas composition, gas pressure, and gas flow rate. Similarly linear thermal expansion is an important characteristic too. Mechanical interactions can arise from a mismatch in thermal expansion between ceramics and structural materials in contact; also cracking can be induced by differential expansion of materials. The cracking and fragmentation of the ceramic materials have to be minimized to avoid difference in the heat transfer throughout the breeder material, which can inhibits the tritium recovery system.

Davis et al. [28] measured the thermal diffusivity and heat capacity of lithium titanate (Li_2TiO_3) ceramic (prepared from commercially available Li_2TiO_3 powder) and from these results thermal conductivity has calculated in the temperature range of 300 to 1000K. All the

samples were 86% dense. The experiments were done by laser flash technique. The thermal conductivity ranged in value from 3 W/mK at 300 K, decreasing to 2.2 W/mK in the 425 to 675 K temperature range, and then increasing to ~ 2.6 W/mK at 1000 K. An increase in thermal conductivity value above 600K is due to the increase in heat capacity.

Saito et al. [29] investigated the effect of density variation and thermal hysteresis on the thermal conductivity, specific heat and thermal expansion of the Li_2TiO_3 pellets from room temperature to 1100K. Density dependence on thermal conductivity was expressed by the modified Maxwel–Eucken equation. Thermal conductivity of the material depends upon the porosity, pore distribution and grain size. Thermal hysteresis of Li_2TiO_3 was not observed during heating and cooling cycles in thermal diffusivity and thermal expansion measurements. Li_2TiO_3 appears to be stable to temperatures between room temperature and 1100 K.

2.4 Tritium release behavior of Li_2TiO_3:

The primary function of a lithium containing ceramics is to breed tritium. The breeder must be maintained within a specified temperature range for acceptable tritium release. Lithium when irradiated with neutron produces tritium. The tritium is then recovered from the surface of the breeder material by a purge gas which contains hydrogen and helium, composition was mainly He+ 0.1% H_2 gas. Tritium generated in the breeder materials primarily by the reaction Li(n, 4He)T, is believed to diffuse across the grain to the grain boundary and then through the grain boundary to the network of interconnected pores and then surface reactions, desorption, and molecular diffusion in the gas phase i.e purge flow convection. [30-32]. At the solid/gas interface between the effective bulk and the pores, tritium desorbs in molecular form as T_2, HT, T_2O and HTO depending on the chemistry of the solid and gas phase in the pores. Once tritium molecules desorb, they percolate through the network of fine pores to a purge stream which take out the tritium out of the breeder material [33]. The fact is that diffusion in the grain and desorption at the pore walls are two most rate-controlling mechanisms regarding tritium release. For better tritium release small grain microstructure and open pore structure is preferred.

2.5 Electrical Conductivity behavior of Li_2TiO_3:

Electrical properties of breeder ceramics are of great importance not only concerning the appearance of electric and magnetic fields in fusion reactors during plasma operations but also regarding the tritium release. If the blanket zone forms a close circuit then the electric and changing magnetic field may cause electric current in the blanket material which leads to change in electrical properties of the sample. Electrical properties may also reflect some characteristic features of the microstructure. [34-36]. Noda et al. [37] suggest that the tritium ion is in the valence state of T^+ and is assumed to be bound with the oxygen ions. The migration of the tritium ions is assumed to occur by hopping from oxygen to oxygen on oxygen lattice. In such migration process the tritium must overcome the barrier of electrostatic repulsion due to lithium ions. Since the lithium ion is consider to migrate through vacancy mechanism, the lithium ion diffusion causes frequent replacement of lithium ion sites by lithium ion vacancy. Hence the repulsive force decreases and the tritium can easily migrate. So higher is the lithium ion conductivity higher will be the tritium diffusion. So, there is a quantitative similarity between lithium movement and tritium migration in solid breeder materials.

Vitins et al. [38] studied the electrical conductivity in the monoclinic Li_2TiO_3 and cubic $Li_{1.33}Ti_{1.67}O_4$ by impedance spectroscopy in the temperature range of 20-730^oC. Li_2TiO_3 shows low lithium ion conductivity, σ_{DC} (573 K)$\sim 10^{-6}\Omega^{-1}$ $cm^{-}1$. The DC conductivity of Li_2TiO_3 certainly depends on the sintering conditions and on non-stoichiometry of the sample. The conductivity of Li_2TiO_3 depends on the temperature. The plot of conductivity ($\log(\sigma T)$) vs temperature (1000/T(K)) is not linear because of the change in conductivity mechanisms (Extrinsic and intrinsic conductivity). A change in slope of $\log \sigma_{DC}T-$ (1/T) was observed between ~775 K–975 K; it was attributed to a first-order phase transition associated probably with order disorder effects and charge transport was presumed to be due to Li+ ions. Li+ migration is thought to occur in the first place in (001) planes of the monoclinic lattice, associated with the presence of lattice defects.

Fehr et al. [39] investigated the conductivity of Li_2TiO_3 specimens having different microstructure and concluded that the impedance spectra change is primarily due to difference in microstructure. Samples were prepared in two different conditions (i) reducing atmosphere (ii) in oxidizing environment. They pointed out the anomalies in DC conductivity at 880 K are due to the presence of high temperature cubic phase of Li_2TiO_3.

References:

1. Kleykamp H., Fusion Eng. Des. 61-62, (2002), 361-366
2. Kleykamp H., J. Nucl. Mater. 295, (2001), 244–248
3. Izquierdo G., West A.R., Mater. Res. Bull. 15 (1980) 1655
4. Mikkelsen J.C., J. Am. Cer. Soc. 63 (1980) 331
5. Landolt-Bornstein N.S., Group III, vol. 7e, Springer, Berlin, 1976
6. Dorrian J.F. and Newnham R.E., Mat. Res. Bull. 4, (1969), 179
7. Lang G., Zeitschrift fur Anorganische und Allgemeine Chemie 276, (1954),7
8. Hodeau J. L., Marezio M., J. Solid State Chem. 45, (1982),170-179
9. Roux N., Avon J., Floreancig A., Mougin J., Rasneur B., Ravel S., J. Nucl. Mater. 233-237, (1996), 1431 – 1435
10. Xiangwei Wu, Zhaoyin Wen, Xiaoxiong Xu, Zhonghua Gu, Xiaohe Xu, J. Nucl. Mater. 373, (2008), 206–211
11. Xiangwei Wu, Zhaoyin Wen , Bin Lin, Xiaogang Xu Mater. Lett. 62, (2008), 837–839
12. Mohammadi M. R., Fray D. J., J Sol-Gel Sci Technol 2010
13. Nguyen M.H., Lee S.J., Kriven W.M., J. Mater. Res. 14, (1999), 3417
14. Lee S.J.,. Kriven W.M, J. Am. Ceram. Soc. 81, (1998), 2605
15. Gulgun M.A., Popoola O.O., Kriven W.M., J. Am. Ceram. Soc. 77, (1994), 531
16. Jung C.H., Lee S.J.,. Kriven W.M., Ji-Yeon Park , Woo-Seog Ryu, J. Nucl. Mater. 373, (2008), 194–198
17. Hoshino T., Sasaki K., Tsuchiya K., Hayashi K., Suzuki A., Hashimoto T., Terai T., J. Nucl. Mater. 386–388, (2009), 1098–1101
18. Chen W., Li F. and Yu J., Mater.Lett., 60, 2006,57–62.
19. Deganello F., Marci G., Deganello G., J. Eur. Cer. Soc. 29 (2009) 439–450
20. Marinsek M., Zupan K. and Maeek J., J. Power Sources, 106, (2002),178–188.
21. Chakroborty A., Das Sharma A., Maiti B. and Maiti H. S., Mater. Lett., 57, 2002,862– 867.
22. Cheng S.Y., Fu S.L., Wei C.C., Ke G.M., J. Mater. Sci. **21,** 571 (1986
23. Jung C.H., Park J.Y., Oh S.J., Park H.K., Kim Y.S., Kim D.K., Kim J.H., J. Nucl. Mater. 253,(1998),203–212
24. Jung C.H., J. Nucl. Mater. 341, (2005), 148–152
25. Jung C.H, Lee S.J, Kriven W. M., Ji-Yeon Park , Woo-Seog Ryu, J. Nucl. Mater. 373, (2008), 194–198

26. Sinha A., Nair S.R., Sinha P.K., J. Nucl. Mater. 399, (2010), 162–166
27. Rhee Y.W, Yang J.H, Kim K.S., Kang K.W., Song K.W., Kim D.J. ,Thermochimica Acta, 455 (2007) 86–89
28. Davis J.W., Haasz A.A., J. Nucl. Mater. 232, (1996), 65-68
29. Saito S., Tsuchiya K., Kawamura H., Terai T., Tanaka S., J. Nucl. Mater. 253, (1998), 213–218
30. Federici G., Wu C.H., Raffray A.R. and Billone M.C., J. Nucl. Mater. 187, (1992), 1-31
31. Kinjyo T., Nishikawa M., Enoeda M., Fukada S., Fusion Eng. Des. 83, (2008), 580–587
32. Raffray A.R., Cho Seungyon, Abdou M.A, J. Nucl. Mater. 210, (1994), 143-160
33. Federici G., Raffray A.R., Billone M.C., Wu C.H., Cho S., Abdou M.A., J. Nucl. Mater. 212-215, (1994), 1003-1009
34. Noda K ., Ishii Y.,Matsui H., Ohno H.and Watanabe H., Fusion Eng. Des. 8, (1989), 329-333
35. Konishi S., Ohno H., Hayashi T., Okhunu K., Matsuo T., Adv Ceram 27,(1990),173-182.
36. Konishi S., Ohno H. J. Nucl. Mater. 152,(1988),9-13
37. Noda K., Ishii Y., Matsui H., Ohno H.,Hirano S. and Watanabe H., J. Nucl. Mater. 155-157, (1988), 568-571
38. Vitins G., Kizane G., Lusis A., Tiliks J., J. Solid State Electrochem. 6, (2002), 311
39. Fehr Th., Schmidbauer E., Solid State Ionics 178, (2007), 35–41

Chapter III

Scope and Objective of Thesis

As discussed in the literature review, lithium titanate (Li_2TiO_3) is a promising candidates for tritium breeding materials in D–T fusion reactors of the ITER test blanket module (TBM) for DEMO reactor because of its reasonable lithium atom density, low activation, excellent tritium release performance and chemical stability. For tritium recovery purpose samples having 85-90% of true density with open porosity (around 5%) is required. Uniform small grain size distribution (having diameter between 2-4μm) is preferable as activation energy for tritium diffusion through grain is higher compared to grain boundary. Solid state method have been used to prepare Li_2TiO_3 powder and followed by sintering. However, large particle size and longer diffusion path require higher calcination temperature there producing coarser particle and impurity, which adversely affects in achieving high sintered density (above 85% of theoretical density). During high temperature sintering this material has tendency to form large grain size and entrapped closed pore inside the grain due to high vapour pressure of lithium oxide and tendency to form liquid phase at higher temperature. As it is clear from the literature review presence of closed pore may significantly affects tritium release from the ceramic during neutron irradiation.

Recently, a novel powder preparation method based on solution combustion synthesis process (SCSP) or auto-combustion technique was developed for the preparation of high purity, active and nano-crystalline Li_2TiO_3 breeder powder for lowering the sintering temperature. But all of them used $TiCl_4$ or Ti-isopropoxide as source of Ti which is costly. There are no report on the effect of different process parameter of solution combustion synthesis process on the particle size and morphology of the powder and its effect on sintering and final microstructure of the ceramic using cheaper precursor of Ti (e.g. TiO2).

The present study aims to investigate the following point.

- Optimization of process parameters (e.g. complextant/fuel to metal ratio, pH of the starting solution, fuel oxidizer ratio) in solution combustion technique using cheaper precursor of Ti (e.g. TiO2) to produce dense ceramic at low temperature. For comparison Li_2TiO_3 will be also prepared by solid state route.
- Effect of various process parameter on the different powder property (e.g. particle size, powder morphology, surface area).

- Effect of powder morphology on the densification behavior and microstructure of the sintered product.
- Comparison of different property (Thermal expansion, thermal conductivity, electrical conductivity) of the sintered ceramic prepared by combustion technique and neutron irradiation behavior of the Li_2TiO_3 powder.

Chapter IV

Experimental Work

4.1 Powder synthesis:

Li_2TiO_3 powder has been synthesized following solution combustion synthesis technique. As discussed in the literature the combustion technique is based on oxidation and redox reaction between an organic fuel and oxidant present in the precursor solution. Generally citric acid, urea, glycine etc. are used as the organic fuel and nitrates of different metals are used as the oxidant. The fuels has dual role, it helps in complex formation with the metal ions and finally on decomposition and oxidation releases enormous amount of heat. It is observed that the exothermic oxidation-reduction reactions of gas-phases which may leads to the development of porous floppy ash. The combustion may be associated with flame or without flame, and the flame temperature can be varied by varying amount of fuel and oxidizer taken, sometimes pH of the precursor solution. Several process parameters have been reported in the literature to control the complex formation and decomposition / self ignition of the gel. In the present work Li_2TiO_3 powder has been synthesized by taking the starting precursor as Li_2CO_3 for lithium source and Ti-nitrate as Ti source. $TiO(NO_3)_2$ was not commercially available and was prepared using precipitation technique. The different experimental techniques used during the present study have been discussed below:

4.1.1 Preparation of $TiO(NO_3)_2$ solution and its estimation:

Titanium dioxide (TiO_2) is generally insoluble in mineral acid, however TiO_2 reacts with the sulphuric acid (H_2SO_4) and forms titanium sulphate. The formation of $TiO(SO_4)$ can be enhanced with the addition of ammonium sulphate $(NH_4)_2SO_4$. The preferred temperature was reported to be 80-90^oC. The preparation of $TiO(NO_3)_2$ solution has been discussed as follows. Weighted amount of TiO_2 [Merck], and $(NH_4)_2SO_4$ [Merck], were mixed with concentrate H_2SO_4 [Merck] and the mixed suspension was heated on hot plate with constant and vigorous stirring until a clear solution was obtained. The dissolution reaction may be written as follows:

$$TiO_2 + H_2SO_4 \rightarrow TiO(SO_4) + H_2O \quad (4.1)$$

The solution was then diluted with addition of distilled water in an ice bath since the acid water reaction is highly exothermic it may leads to precipitation. Ammonium hydroxide (NH_4OH) [Merck] was added to chilled solution with constant stirring, wherein a white precipitate was formed. The possible reaction for the formation of precipitate may be written as

$$TiO(SO_4) + 2NH_4OH \rightarrow TiO(OH)_2 \downarrow + (NH)_2SO_4 \quad (4.2)$$

The precipitate was washed repeatedly with distilled water to make it sulphate free. Then, the washed white precipitate was dissolved in dilute nitric acid (HNO_3) [Merck], (HNO_3: H_2O = 1:1). The possible reaction may be written as

$$TiO(OH)_2 + 2HNO_3 \rightarrow TiO(NO_3)_2 + 2H_2O \quad (4.3)$$

Thus the $TiO(NO_3)_2$ had been prepared for the present study. TiO_2 content of the $TiO(NO_3)_2$ solution thus prepared has been estimated using gravimetric technique. The schematic flow chart of titanium nitrate solution preparation was shown in Fig. 4.1.

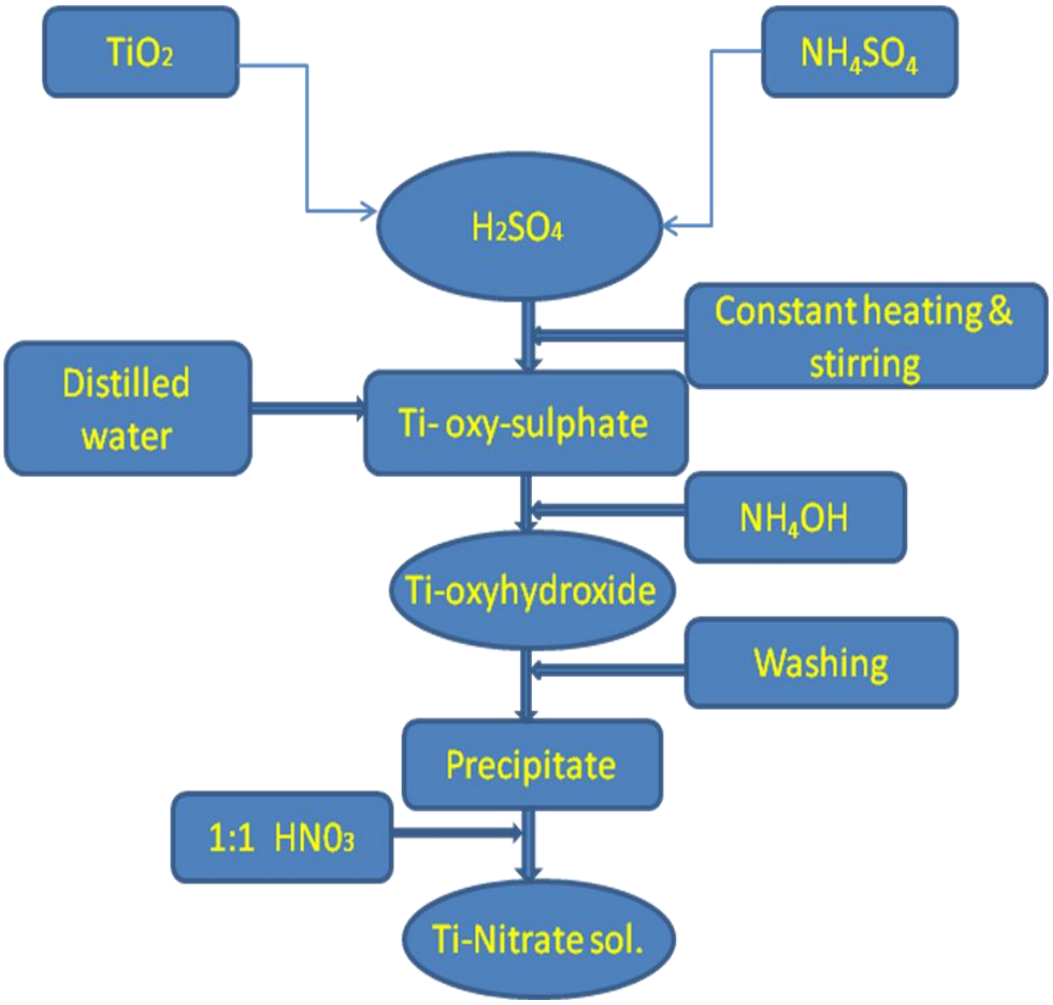

Fig. 4.1 Schematic representation of preparation of titanium nitrate solution

4.1.2 Combustion Synthesis of Li_2TiO_3:

The starting precursors for the preparation of Li_2TiO_3 taken were Lithium carbonate (Qualigens, 98.5%), titanium oxy-nitrate and citric acid (CA, Merck, 99 %). Citric acid plays the role of fuel as well as complexing agent. Citric acid ($C_6H_8O_7$) has three carboxylic and one hydroxyl group for coordinating to metal ions and therefore prevents precipitation or phase segregation, thus providing an intimate blending among constituent ions [1]. It is a low cost material and can be combusted with carbonates and nitrates (i.e. oxidant) at low ignition temperature (200–250^oC), and hence is a good choice as a fuel in the combustion technique [2]. Another role of citric acid is it acts as complexing agent to the metal ions. We have chosen citrate to metal ratio, which was optimized to get uniform and complete combustion. The molar ratios of the citrate to metal were kept at 0.8 (LT1), 1 (LT2), and 1.5 (LT3) and the corresponding citrate to nitrate ratio were 0.07, 0.09 and 0.13 respectively. In all the cases pH of the starting solution were at 1.

Stoichiometric amount of Li_2CO_3, $TiO(NO_3)_2$ were mixed along with citric acid and heated at 80-100^oC with constant stirring on hot plate. NH_4OH solution (Merck, 25%) was then added drop by drop under constant stirring in order to adjust the pH. The pH of the starting solution was 1 and was varied from 1 to 6 to see the combustion behavior and powder morphology. The schematic flow chart of sample preparation was shown in Fig. 4.2. The combustion for pH=1 is slow and flameless (Fig.4.3(a)), however samples prepared at higher pH are vigorous and highly exothermic (Fig. 4.3(c).The as-burnt powder was calcined at 600°C for 2 hrs to get better crystallization and finally ground to get Li_2TiO_3 breeder powder. For comparison samples of Li_2TiO_3 were also prepared by solid state reaction route. The stoichiometric amount of Li_2CO_3 (Qualigens, 98.5%) and TiO_2 (Merck, 99 %) were taken and ball milled in iso propyl alcohol solvent. 15mm diameter Zirconia balls were used as grinding media.

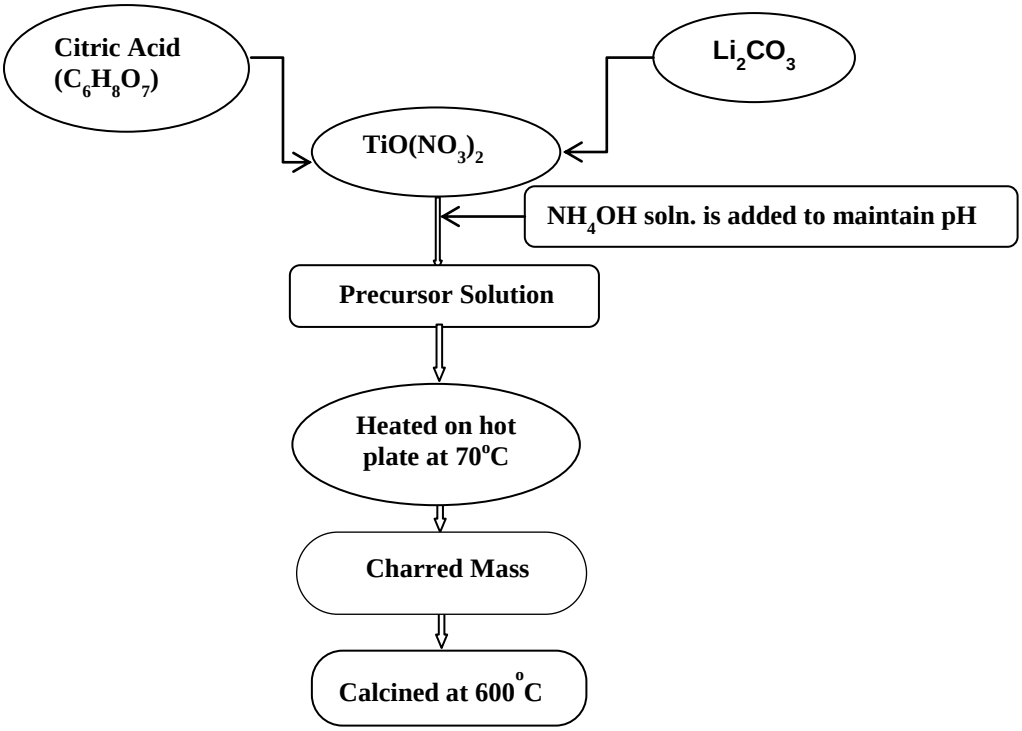

Fig. 4.2 Flow chart for preparation of Li_2TiO_3 powder

Fig. 4.3 Photographs of citrate-nitrate solution (a) pH=1 (b) auto combustion reaction (pH=1) (c) pH=3and (d) as burnt powder (pH=3).

4.2 Characterization of Dried Gel and Powder:

4.2.1 Thermal Analysis:

The gel was collected prior the combustion and the dried gel was characterized by differential scanning calorimeter (DSC) and thermo gravimetric analysis (TGA) using NETZSCH STA (Model No 409C). DSC is the more recent technique and was developed for quantitative calorimetric measurements. The signal from the differential scanning calorimeter will be regarded as proportional to the difference in thermal power between the sample and reference, $d\Delta q/dt$. Differential scanning calorimeters make use of a crucible to contain the sample. The reference is either an inert material in a crucible of the same type as that used for the sample or simply the empty crucible. Crucibles commonly measure 5-6 mm in diameter made up of alumina. This technique is excellent for determining the chemical kinetics, enthalpy transitions and transformation, presence and quantity of hydrated water, decomposition behavior of gel, phase transitions, crystallization temperature and formation of products, etc. of precursor powders synthesized through different chemical route. Thermal analysis of dried gel was carried out in air atmosphere with the heating rate of 10^{o}C/min from RT to 1000^{o}C. When a material undergoes physical or chemical change it absorbs or releases thermal energy. The temperature difference of the sample with respect to the reference inert material (α-Al2O3) during heating or cooling is plotted in a DSC curve as the deviation from zero base line. Exothermic or endothermic changes are shown in opposite directions of the baseline.

Theory of DSC:

The aim was to derive an expression for the instrument signal in response to the evolution of heat from a sample as represented by dh/dt. The sample and its crucible were considered as one with a total heat capacity C_P. A similar assumption was made regarding the reference material and its crucible, which together had a total heat capacity C_R. It was assumed that there is a source of thermal energy at temperature Tp and a single thermal impedance R between the sample and the source of thermal energy and between the reference and the source of thermal energy. The heat flow between the thermal energy source and the sample was represented as dq/dt as measured by the instrument. The heating rate was represented by dT,/dt = p and assumed to be linear. Gray obtained the equation,

$$\mathbf{dh/dt = - dq/dt + (C_S - C_R)\, dT_P/dt - RC_S\, d^2q/dt^2}. \qquad (4.4)$$

Thus the heat evolution from the sample is given by the instrument signal measured from zero (term 1), a heat capacity displacement (term 2) and a third term which includes the product RC. This product has units of time so that (term 3) represents a thermal lag. Included in the publication was a recipe for obtaining dh/dt from the experimental curve by making allowance for thermal lag. For inert samples dh/dt = 0 and the displacement (term 2) provides a route to the determination of heat capacity.

TGA is basically a analytical technique in which the mass change of a substance is measured as a function of temperature whilst the substance is subjected to a controlled temperature programme. The temperature programme must be taken to include holding the sample at a constant temperature other than ambient, when the mass change is measured against time. Mass loss is only seen if a process occurs where a volatile component is lost. There are, of course, reactions that may take place with no mass loss. As materials are heated, they can lose weight due to drying, or from chemical reactions that liberate gasses. Some materials can gain weight by reacting with the atmosphere in the testing environment. The results may be reported directly as mass of the sample varying with temperature or time, i.e. as m versus T. Thus a mass loss appears as a downwards curve. Instead of mass in mg, the scale may be converted into percent of the original mass. An alternative is to convert the results into a percentage mass loss.

4.2.2 Crystallite Size and Phase Analysis

Phase formation of as burnt and calcined powder samples were studied by the powder X-ray diffraction performed with a Philip's Diffractometer (model: PW-1830, Philips, Netherlands) using Cu Kα radiation. This technique gives some valuable information like crystal structure, crystalinity of the material, crystallite size, chemical analysis etc.The generator voltage and current was set at 35KV and 25mA respectively. The scan rate was 0.04^{o}/sec. the phases present has been identified with the search match facility available with Philips X'pert high score software. A powdered sample is packed on a sample stage so that it can be scanned by the X-ray.

The diffracted X-rays were detected by an electronic detector placed on the other side of the sample. To get the diffracted beams the sample was rotated through different Bragg's angles. The goniometer keeps track of the angle (θ), and the detector records the detected X-rays in

units of counts/sec and sends this information to the computer. After scan of the sample, the X-ray intensity (counts/sec) (Y axes) was plotted against the angle theta (2θ)(X-axes). The angle (2θ) for each diffraction peak was then converted to d-spacing, using the Bragg's law;

$$\mathbf{n\lambda = 2d\ Sin\theta} \tag{4.5}$$

where λ = wave length of x-ray

n = order of diffraction.

The crystallite sizes of the as burnt and calcined powder samples were determined from X-ray line broadening using the Sherrer's equation [3] as follows:

$$t = {}^{0.9\lambda}/_{\beta cos\theta} \tag{4.6}$$

where, t is the crystallite size, λ is the wavelength of the radiation, θ is the Bragg's angle and β is the full width at half maximum. Line broadening due to instrument was subtracted from the peak width before calculating the crystallite size using the following formula:

$$\beta^2 = \beta^2_{obs} - \beta^2_{stan} \tag{4.7}$$

where, β_{obs} = measured full width at half maximum from peak, β_{stan}= instrumental broadening [Standard Silicon sample was used, whose β_{stan} value was 0.09821 at 2θ =29° with (hkl) value (111)].

4.2.3 Surface Area Measurement

Surface area of ceramic powder is an important parameter to predict sintering characteristics. This can be measured by BET (Brunauer, Emmet and Teller after the developers of the basic calculations) method. The BET method involves adsorbing a monolayer of nitrogen gas onto the surface of particles, then measuring the amount of nitrogen that is released when that monolayer is vaporized. Based on this nitrogen quantity adsorbed, the surface area of the sample can be calculated from the BET equation:

$$\frac{1}{V_g}\ \frac{x}{1-x} = \frac{(c-1)}{cV_m}x + \frac{1}{cV_m} \tag{4.8}$$

where, V_g = volume of gas adsorbed, V_m = volume of gas adsorbed at monolayer coverage, x = P/Po, P = Ambient pressure, Po = Total pressure, c = a constant that is related to the heat of adsorption. A plot of $[(1/V_g)(x/(1-x))]$ versus x gives a straight line with slope = m = (c-1)/(cVm), Intercept = g = $1/cV_m$, The value of V_m and c are worked out, V_m = 1/(slope +

intercept). This is normalized by the mass of particles tested to give a specific surface area (m^2/gm).

BET surface area of raw combustion powder as well calcined powder was measured using 5 point method by AUTOSORB 1, (Quantachrome) (Model No: Nova 1200 BET).. The average particle size was estimated by assuming all the particles to have the same spherical shape and size. The average particle diameter, D (in nm), is given by:

$$D = \frac{6000}{S_p * \rho} \tag{4.9}$$

Where "S_{sp}" is the specific surface in m^2/g of the sample and "ρ" is the true density in g/cc.

4.2.4 Particle Size Analysis:

A laser diffraction method with a multiple scattering technique has been used to determine the particle size distribution of the powder. Dispersed particles momentarily traversing a collimated light beam will cause Fraunhofer diffraction of light outside of the cross section of the beam when the particles are larger than the wavelength of the light. The intensity of the forward-diffracted light is proportional to the particle size squared, but the diffraction angle varies inversely with particle size. A He-Ne laser is commonly used for the light source. The combination of an optical filter, lens, and photo detector or a lens and multi element detector coupled with a computer enables computation of the particle size distribution from the diffraction data. The sample may be either a liquid or gas suspension of particles or droplets of about 0.1 vol % concentration. It is based on Mie-scattering theory. In order to find out the particles size distribution the Li_2TiO_3 powder was dispersed in water by horn type ultrasonic processor [Ultrasonic Processor Sonopros, PR1000 MP].Then experiment was carried out in computer controlled particle size analyzer [ZETA Sizers Nanoseries (Malvern Instruments Nano ZS)] to find out the particles size distribution.

4.3 Densification Study of powder compact:

Shrinkage behavior of the green compact and thermal expansion of sintered bar shaped samples were investigated by NETZSCH dilatometer model DIL 402 C. In the dilatometer the specimen is kept in a specimen holder in the centre of the furnace. The linear dimensional

change i.e. shrinkage or expansion of the specimen is transmitted through the push rod (pressed against the sample inside the furnace) to the measuring head.

Samples size was bar having diameter 6 mm and length 15 mm for dilatometer experiment. The heating rate was maintained at 10^{o}C/min. The measurement was carried out from room temperature to 1100^{o}C in air atmosphere.

4.4 Preparation of Bulk Sample:

Calcined powder was mixed with 1-3 wt. % PVA (Poly Vinyl Alcohol) binder with the help of mortar and pestle. The binder mixed powder was compacted to give a desired shape for further characterization. The binder mixed powder was dried and granulated. The granules were uniaxially pressed using a hydraulic press at a pressure of 275 MPa for 2 minutes in a hydraulic press (4T, Carver Inc ,USA) to form cylindrical pellets (Dia-12.5 mm, thickness-2 mm). Some samples were pressed for thermal conductivity measurement having diameter 25mm and height 7mm in a cylindrical die of dimension 25mm diameter and 500mm height. Green densities were calculated from weight/volume ratio. Weight was measured using electronic balance whereas; volume was calculated from the dimension of the specimens.

Sintering study:

Sintering of green compacts was carried out `in a chamber furnace (45R5Y) by heating it from room temperature to 650^{o}C at a heating rate of 3^{o}C/minute with a holding time of 30 minute at 650^{o}C for binder removal. Thereafter, the heating was continued at the rate of 3^{o}C/minute till the final sintering temperature was attained. A holding time was provided at the peak sintering temperature. Following the sintering, the samples were furnace cooled to room temperature.

4.5 Density and apparent porosity:

Bulk density and apparent porosity of sinter specimens were determined by Archimedes principle. Sintered samples were weighted in dry state. Samples were immersed in kerosene and kept under a vacuum desiccators 4 hrs to ensure that kerosene filled up the open pores completely. Then, soaked and suspended weights were measured. The apparent porosity and bulk density were calculated as follows:

W_d =Dry weight of the sample,

W_s = Soaked weight of the sample,

W_a =Suspended weight of the sample

$$\text{Bulk density} = \frac{W_d}{W_s - W_a} * \text{Density of kerosene} \quad (4.10)$$

$$\text{Apparent porosity} = \frac{W_s - W_d}{W_s - W_a} * 100 \quad (4.11)$$

4.6 Microstructural analysis:

Microstructural analysis is one of the important interpretation tool regarding the tritium release property of breeder material. For tritium recovery purpose we need samples having 85-90% of TD with a significant open porosity of 5%. Again Uniform grain size distribution having diameter between 2-4μm is required for this purpose.

In the SEM, a source of electrons is focused (in vacuum) into a fine probe that is rastered over the surface of the specimen. As the electrons penetrate the surface, a number of interactions occur that can result in the emission of electrons or photons from (or through) the surface. A reasonable fraction of the electrons emitted can be collected by appropriate detectors, and the output can be used to modulate the brightness of a cathode ray tube (CRT) whose x- and y inputs are driven in synchronism with the x-y voltages rastering the electron beam. In this way an image is produced on the CRT; every point that the beam strikes on the sample is mapped directly onto a corresponding point on the screen.

As fired samples and the fractured surface were cleaned in acetone and dried at 100^{o}C for 24hr for SEM imaging. Some sample surfaces were polished on fine emery paper; the samples were thermally etched at 50^{o}C less than the sintering temperature. Powder samples were dispersed in water medium in ultrasonic vibrator (Oscar, Sonopros PR-1000MP). One drop was put on a glass plate and dried under IR lamp for 4 hr prior to the SEM imaging.

4.7 Electrical conductivity measurements:

For electrical characterization the sintered pellets were polished by fine emery paper to make their faces smooth and parallel. Samples were painted by conducting silver paste on the parallel surfaces followed by curing at 500^{o}C for 30 minutes. The AC resistivity ρ was calculated using the formula

$$\rho = RL/A \quad (4.12)$$

Where R= Resistivity

L= Thickness of sample

A=Area of cross section

The conductivity was calculated by taking the inverse of ρ

At low fields, this means at average applied fields F (i.e., the applied voltage V divided by the specimen thickness d) lower than the threshold (or critical) field F_{th} for switching on significant injection of carriers from the carrier injecting contacts. Electrical conductivity follows the empirical equation given by

$$\sigma = \sigma_o \exp(-Ea/kT) \quad (4.13)$$

Where σ_o is the pre exponential factor and Ea is the activation energy, k is Boltzmann's constant and T is temperature in Kelvin.

4.8 Thermal Conductivity measurement:

Several techniques are used to measure thermal conductivity (k_{th}) in solids. One method that has gained popularity recently is the laser flash technique. This technique attempts to measure the time evolution of the temperature on one side of the sample as the other side is very rapidly heated by a laser pulse. As it passes through the solid, the signal will be altered in two ways: There will be a time lag between the time at which the solid was pulsed and the maximum in the response. This time lag is directly proportional to the thermal diffusivity (α), of the material. The second effect will be a reduction in the temperature spike, which is directly related to the heat capacity (c_p) of the solid. The heat capacity, thermal diffusivity , and thermal conductivity and density are related by:

$$K_{th} = \rho C p \alpha \quad (4.14)$$

The conduction of heat through solids occurs as a result of temperature gradients. Thermal energy in solids is transported by lattice vibrations, i.e. phonons, free electrons, and radiation. In ceramics the concentration of free electrons is very less thus the phonon mechanism virtually responsible for the thermal conduction. When a solid is heated, the atoms in that region will have large amplitudes of vibration and will vibrate violently around their average positions. This sets the neighboring atoms into oscillation. As a result the disturbance, caused by the application of heat, propagates outward in a wavelike manner. These waves, in complete analogy to electromagnetic waves, can be scattered by imperfections, grain boundaries and pores or even reflected at other internal surfaces. So thermal conductivity depends upon several parameters, which can be controlled by adopting new processing steps.

References:

1. Tsay J.and Fang T., J. Am. Ceram. Soc., 1999, 82, 1409.
2. Schafer J., Sigmund W., Roy S.and Aldinger F., J. Mater. Res., 12, (1997), 2518.
3. Cullity B. D., 'Elements of X-Ray Diffraction', 2nd Ed, Addision-Wesley. INC (1978).

Chapter V

Results and discussions

RESULTS AND DISCUSSIONS:

5.1 Optimization of Process Parameters for Synthesis of Li_2TiO_3:

The solution based auto combustion technique is a novel way with a unique combination of the sol-gel process and the combustion process. However it is sensitive to the amount of oxidizer, reducer, complexing agent and pH. Optimization of different process parameters namely citric acid, and pH on the phase formation of pure Li_2TiO_3 powder have been discussed below:

5.1.1 Optimization of citrate to metal (C/M) ratio:

The molar ratios of the citrate to metal (C/M) were kept at 0.8 (LT1), 1 (LT2), and 1.5 (LT3). The corresponding citrates to nitrate (C/N) ratios were 0.07, 0.09 and 0.13 respectively. In all the cases pH of the starting solution were at 1. It was found that precipitation was occurring during heating and evaporation of the gel for metal to citrate ratios below 0.8. Here citric acid has dual role it acts as a complexant for metal ions and fuel for combustion reaction. At low citric acid content chelation was poor and some metal ions like titanium remains free in the solution and reacts with oxygen to form precipitate of titanium dioxide.

Fig. 5.1 (a-c) shows the XRD patterns of the powders calcined at different temperature for LT1, LT2 and LT3. It has been observed that the phase purity temperature depends on the metal to citrate ratio. The phase formation temperature for LT1 samples was found to be at 700^oC. At low temperature i.e at 500^oC the amorphous nature can be easily seen from XRD. Whereas at 600^oC the impurity phases of $Li_2Ti_4O_9$ were found. So the phase pure crystalline powder was obtained at 700^oC (Fig. 5.1(a)). Similarly for the samples LT2 and LT3, the phase formation temperature noticed to be 600^oC/2hrs. Samples heat treated at 500^oC shows impurity phases of $Li_2Ti_4O_9$ as in case of LT1 and LT2 (Fig. 5.1 ((b), (c)).

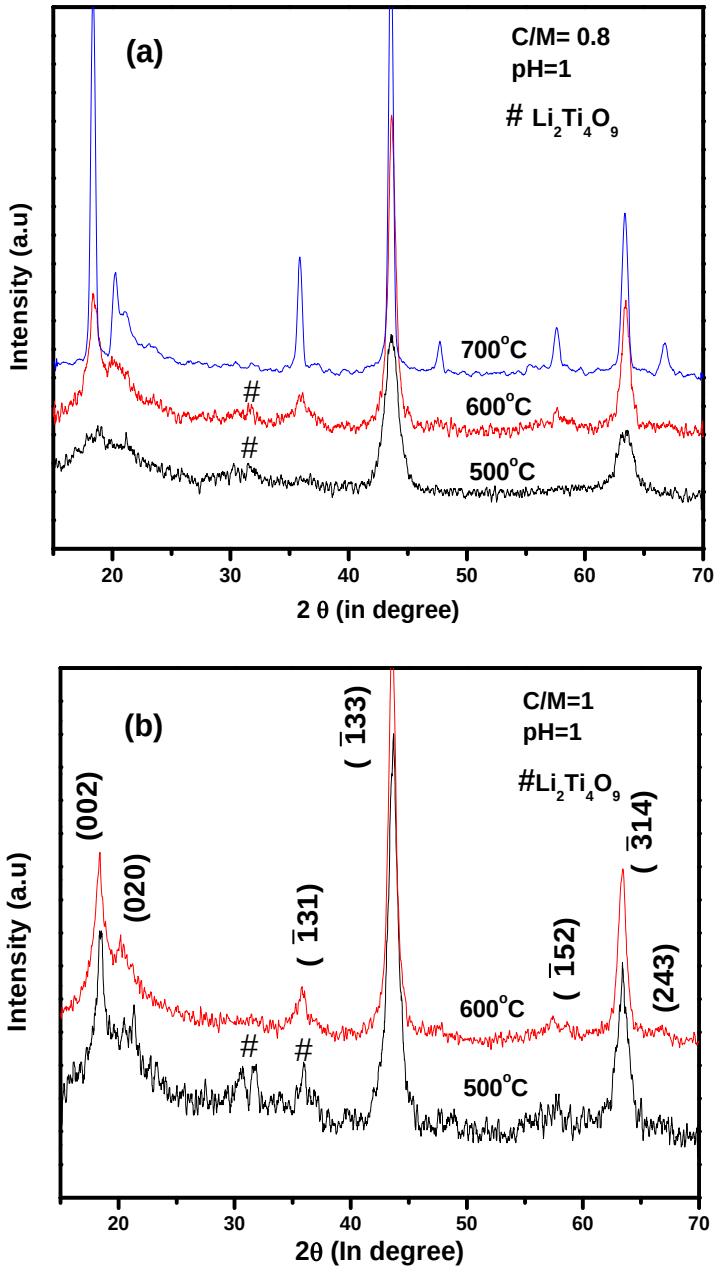

Fig 5.1 XRD pattern of Li_2TiO_3 calcined at different temperature for C/M (a) 0.8 and (b) 1

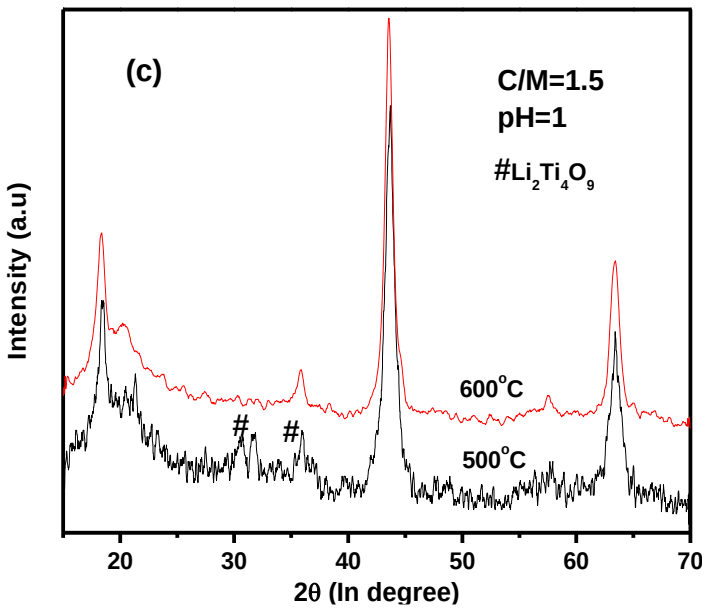

Fig. 5.1 (c) XRD pattern of Li_2TiO_3 calcined at different temperature for C/M=1.5

5.1.2 pH variation:

In the previous chapter (No.2) we have discuss how pH variation of the starting solution of other system can greatly modify the phase purity or phase formation temperature and morphology of the powder. Here we are interested to study the combustion behavior of the gel and powder morphology by varying the pH (1, 3 and 6) of the starting solution by using ammonia solution. For this study C/M ratio 1 and 1.5 can be considered to be a good choice, since phase formation occurs at lower temperature.

5.3 Phase analysis of as-synthesized and calcined powder:

Fig. 5.2 (a-b) and Fig. 5.3 (a-b) shows the XRD patterns of as-burnt (after autocombustion) and calcined powders for C/M ratios 1 and 1.5 respectively for varying pH. The X-ray diffraction analyses of the as-prepared powder showed that the as-generated powders for both LT2 and LT3 prepared at pH=1 partially crystalline in nature. The diffracted peaks were not sharp but relatively broad, which indicates the amorphous nature of the as synthesized powder and high intensity peaks found only after calcining at 600^{o}C. For both C/M ratio, which is formed at pH 3 and 6 respectively, showed the formation of phase pure and highly crystalline Li_2TiO_3 at the

as-burnt state though it contained a very small amount of carbonaceous material as evident from the grayish color of the powder. It was so calcined at 600^{o}C to remove the residual carbonaceous material.

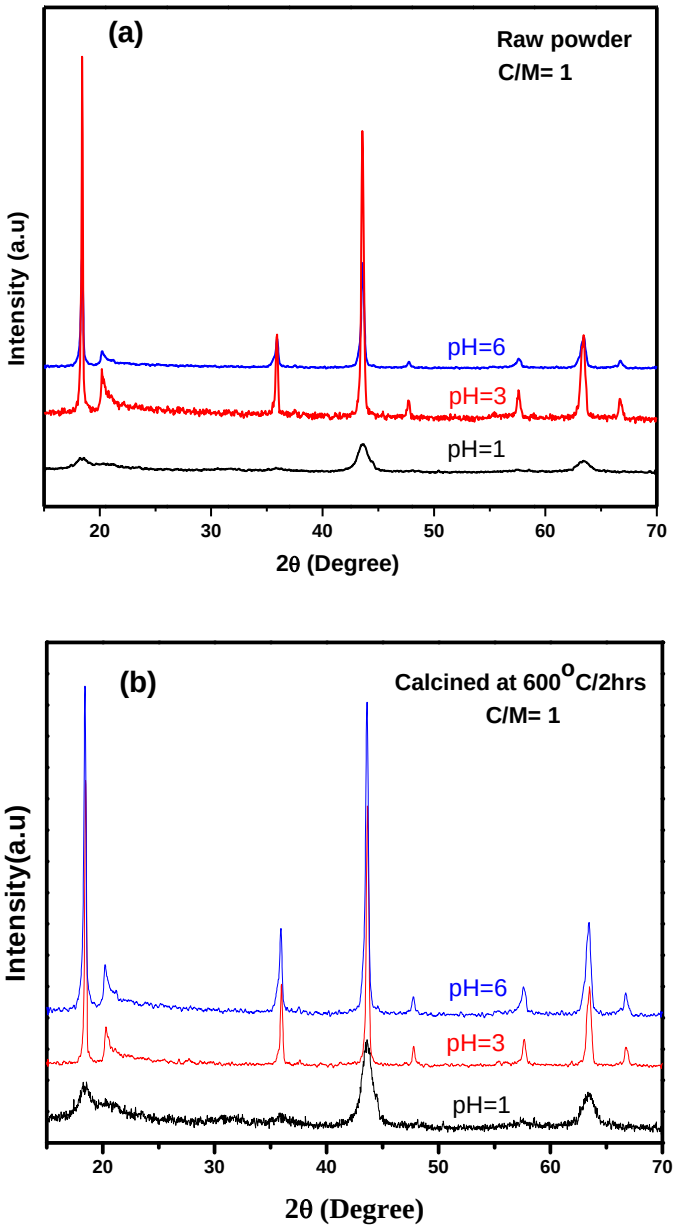

Fig. 5.2 X-Ray diffractogram of Li_2TiO_3 with C/M=1 for different pH of (a) as synthesized and (b) 600^{o}C calcined

X-ray diffraction pattern identification revealed formation of monoclinic phase (JCPDS card number 33-0381) for the LT2 sample with lattice parameter a=5.11Å, b=8.74 Å, c=9.80 Å and β =100.8^{o}. These values were in good agreement with the reported values reported by Kleykamp et.al. [1]. For pH3LT3 the lattice parameters were found to be a=5.03 Å, b=8.82 Å, c= 9.97 Å and β=99.89^{o}.

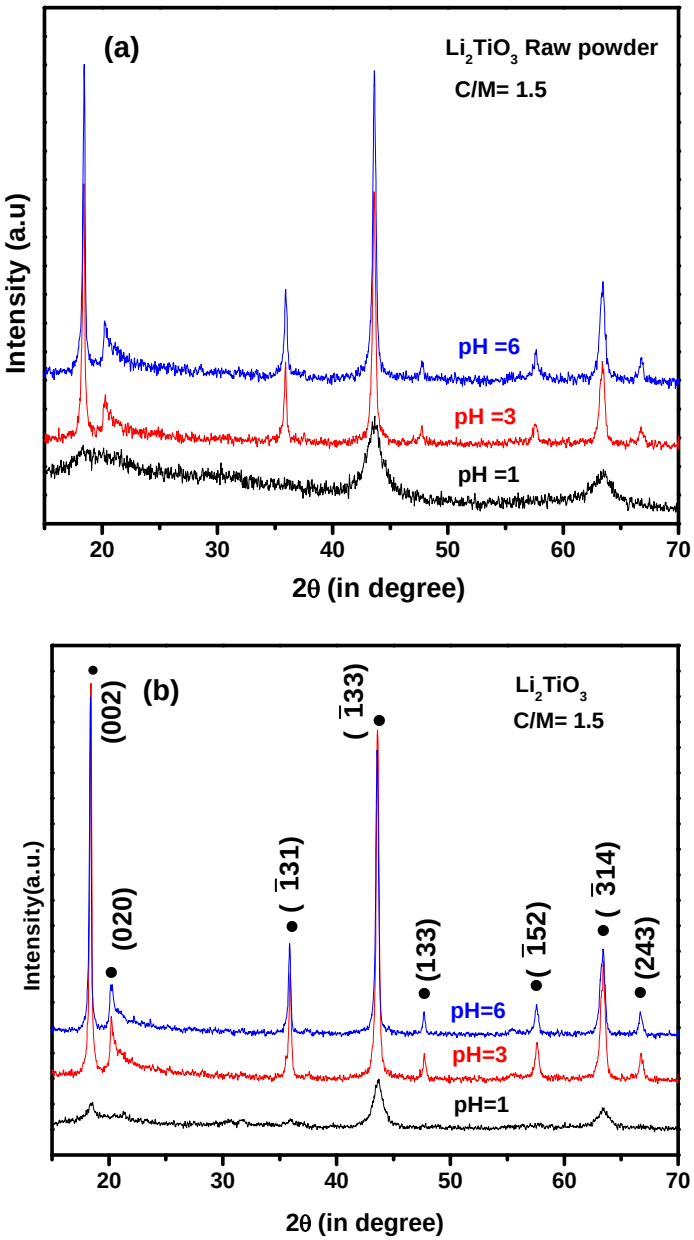

Fig. 5.3 X-Ray diffractogram of Li_2TiO_3 with C/M=1.5 at different pH (a) as synthesized and (b) 600^{o}C calcined

For comparison Li_2TiO_3 was synthesize by the solid state route by ball milling. The solid state derived powder generally required high temperature for phase formation, since diffusion of ionic and atomic species takes place through reactant and product layer. The raw powders were heat treated at 600°C and 700°C for 2 hrs in order to get the desired phase.

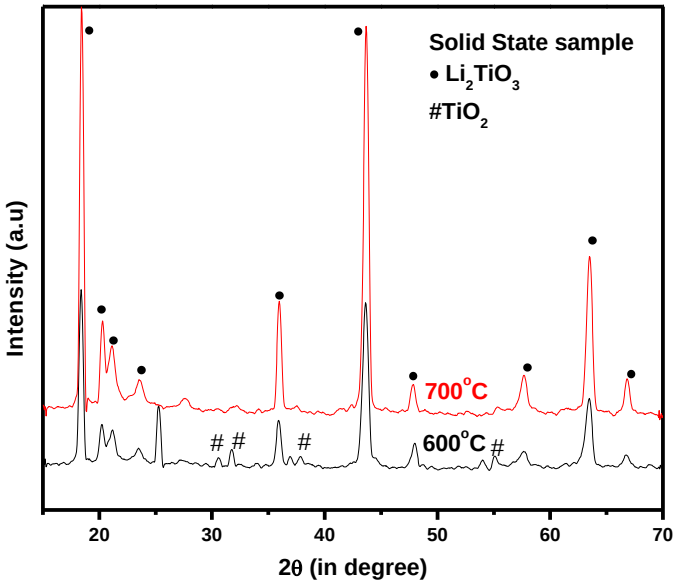

Fig. 5.4 X-Ray diffractogram of Li_2TiO_3 powder synthesized by solid state route and calcined at two different temperature 600°C & 700°C

Fig. 5.4 shows that the 600°C calcined powder contains impurity peaks of unreacted TiO_2 but the phase pure powder was obtained when calcined at 700°C. This high reaction temperature often results in larger crystallite and particle size which affects the sintering of compact body.

5.4 Crystallite size and surface area measurements:

The crystallite size was calculated from X-ray diffraction patterns using Scherer formula of as-synthesized and calcined powder described in chapter (IV). Table -1 summarizes the effect of C/M ratio and pH of the starting solution on the crystallite size, BET surface area, and combustion characteristic of gel. The crystallite size of calcined powders was 12 and 20 nm for LT2 and LT3 sample respectively. Fig. 5.5 shows the variation of crystallite size with pH of the starting solution. It was observed that the crystallite size was increasing with increase in pH of the starting solution. It is known that increase in pH increases the exothermicity of the combustion reaction and that may contribute to increase in crystallite size. It can be observed

from the table that LT2 has highest surface area (62 m^2/gm). It may be due two reason one is lower particle size of powder (shown in micrograph 5.6(a)) and fluffy porous nature of the powder. As we know, a great deal of organic material is decomposed and a strong redox reaction is completed in a short time. These releases a lot of gas can promote the formation of pores.

This is also clear from the table 5.1 that increase in pH reduces the BET surface area of powder. Higher pH shifts the ignition temperature to higher side and that may produce fusion of the particle and formation of hard agglomerate, which reduces the surface area of the generated powder.

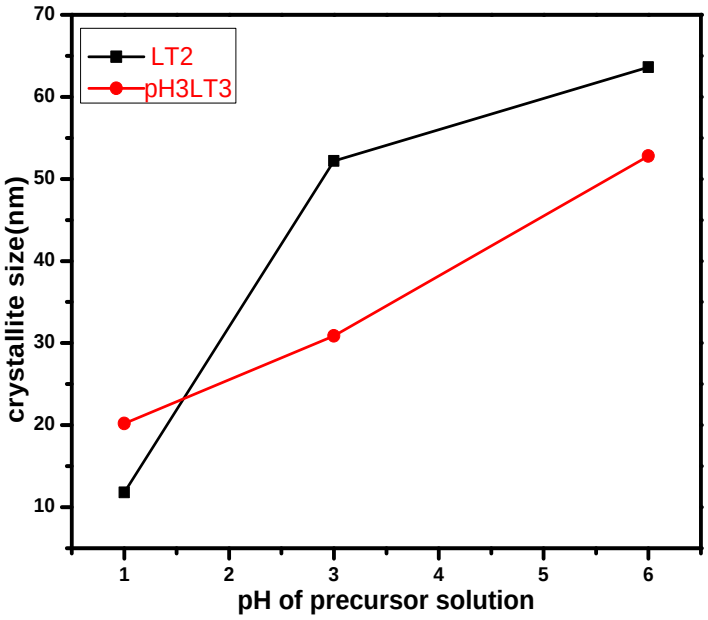

Fig. 5.5 Effect of pH variation on crystallite size of Li_2TiO_3 for two different C/M ratio

Table 5.1: Effect of pH and C/M ratio on surface area, crystallite size and combustion behavior

Sample ID	C /M	BET surface area (m^2/gm)	Crystallite size (nm) from XRD	Observation during combustion
Li_2TiO_3 pH=1**(LT1)**	0.7	-----	-----	Precipitation or Phase separation
Li_2TiO_3 pH=1**(LT2)**	1	62.45	11.8	No phase separation, viscous yellowish gel
Li_2TiO_3 pH=3**(LT3)**	1	34.2	52.2	No phase separation, viscous yellowish gel
Li_2TiO_3 pH=6	1	25.4	63.6	No phase separation, viscous yellowish gel
Li_2TiO_3 pH=1	1.5	35	20.2	No phase separation Blackish gel
Li_2TiO_3 pH=3 **(pH3LT3)**	1.5	40	30.89	No phase separation Blackish gel
Li_2TiO_3 pH=6	1.5	27.2	52.78	No phase separation, viscous yellowish gel
Solid state	-	10.55	41.6	---------

5.5 Morphology of combustion derived powders:

Fig. 5.6 (a),(b) shows the powder morphology of Li_2TiO_3 samples prepared by auto-combustion technique. From fig.5.6 (a) it is clear that LT2 sample has particle size in the range of 100-200 nm whereas pH3LT3 has particle size in the range of 400-500 nm. As previous illustrated, the reaction in higher pH is more exothermic and complete, which means a higher reaction temperature, and that enhancing the particle size and formation of hard agglomerates.

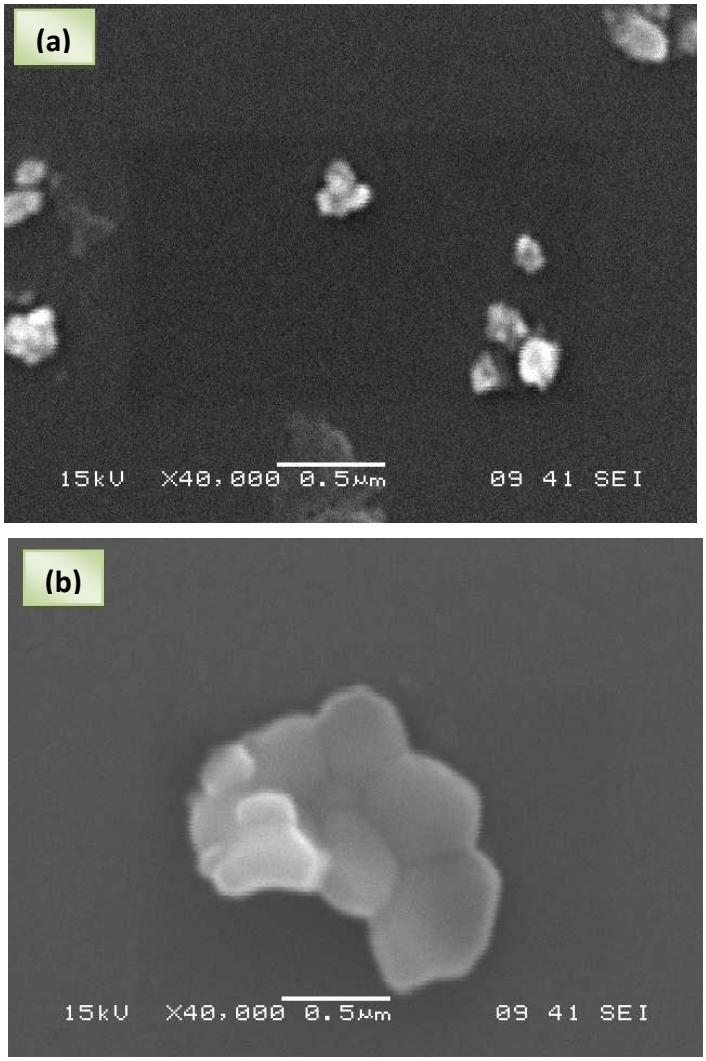

Fig. 5.6 SEM micrograph of calcined powder sample (a) LT2 and (b) pH3LT3

5.6 ICPS analysis of the powder samples:

Inductively Coupled Plasma Atomic Emission Spectrometer (ICPS) analysis shows the presence of different elements. The results are summarized in Table 5.2. It is clear from the table powder sample contains small amount of Al impurity which is a neutron absorber. In order to confirm the presence of aluminum neutron activation studies were carried out in later stage.

Table 5.2 Different wt% of elements in Li_2TiO_3 Powder:

Sl.no.	Element	Wt%
1	Li	10.9
2	Ti	42.25
3	Al	0.3
4	Fe	0.07
5	K	0.03
6	Ni	0.0028
7	O	46.447

5.7 Thermal analysis of gels:

Fig. 5.7 depicts the DSC-TG of the gels having different citrate to metal ratio. All the samples show double stage decomposition. The first exotherm can be assigned to the decomposition of the metal complexes, and the second peak can be attributed to the oxidation of the residual carbonaceous mass along with slow crystallization of the amorphous structure [2]. A weight loss of more than 50% was noticed around the first exothermic peak. It is interesting to note that intensity of exothermic peak occurred at 170^{o}C, or exothermicity of the reaction decreases with higher C/M which is also corresponds to higher citrate to nitrate ratio or fuel/oxidant ratio. This can be explained from the redox reaction between the citrate ions and the nitrate ions present in the solution. The activation of the fuel depends on the presence of nitrate ions, so an increase in the citrate ions decreases the availability of nitrate ion for activation. This results in the decrease in intensity of combustion reaction [3].

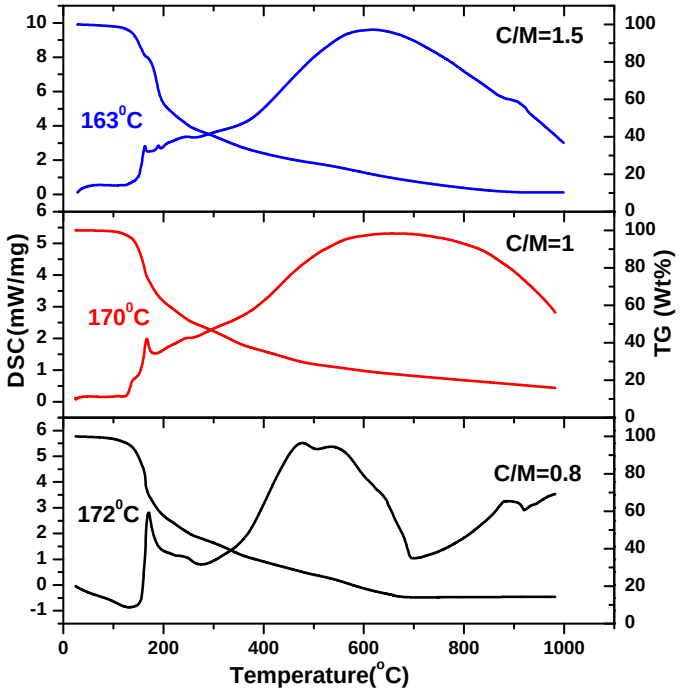

Fig. 5.7 DSC –TG graph of gels for different C/M ratio prepared at pH=1

Fig. 5.8 (a-b) shows the DSC-TG of dried gels for LT2 sample which was synthesized at different pH. It was observed that the combustion rate is influenced significantly by the pH value of the mixed solution. With increasing pH value from 1 to 6, the combustion rate increases.

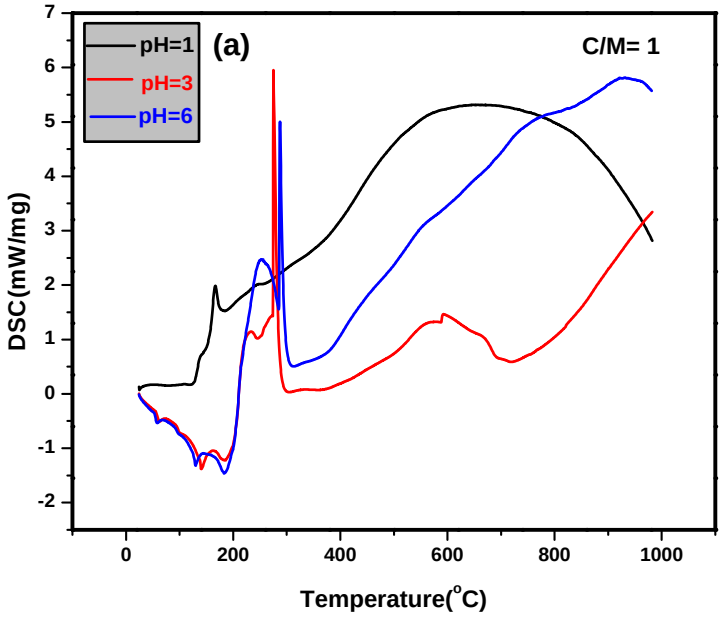

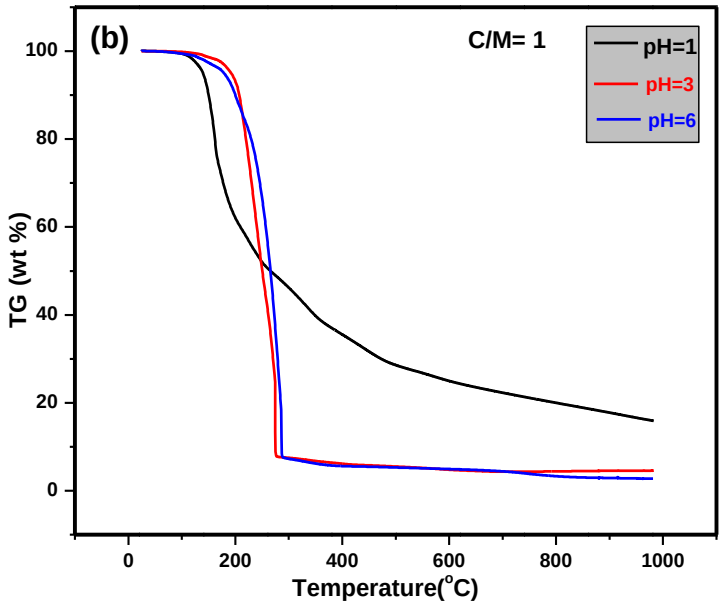

Fig. 5.8 (a) DSC curves of the gels for C/M= 1 and for different pH=1,3&6
(b) TG curves of the gels for C/M= 1 and for different pH=1,3&6

It is interesting to note that in LT2 sample for pH 3 and 6 the decomposition is almost single step and combustion reaction which associated with more than 85% weight loss at around 275^{o}C (pH =3) and drops down quickly. The enthalpy changes are 60, 337 and 393 J/gm for pH 1, 3, 6 respectively. Strong exothermic peaks were seen for both batches at around 270-280^{o}C which is associated with the redox reactions of burning the chemical groups involved in nitrate–citrate anions. But it contains another small exothermic peak around 600^{o}C without any significant weight change may be due to the crystallization process. It is a relatively slow process and the associated total enthalpy change (area under the peak) is rather large. The endothermic peaks at around 138^{o}C (for pH 3) and 123^{o}C (for pH 6) may be attributed with the physically adsorbed water present in the dehydrated gel. The endothermic peaks at temperature 181^{o}C may be due to the decomposition of the small amount of excess citric acid present in the gel network [2].

Fig. 5.9(a-b) shows the DSC-TG of dried gels for LT3 sample which was synthesized at different pH. The samples with ratio C/M =1.5 prepared at pH=3 and 6 are designated as pH3LT3, pH6LT3. As the citric acid amount increased the citrate to nitrate (C/N) ratio become higher. Higher C/N ratios result in lower intensity of the auto-combustion reaction, as already

observed by other authors [4]. It is clear from the DSC-TG curve for pH3LT3, pH6LT3 respectively. As described earlier the intensity of the reaction was lowered in both the cases as concluded from DSC. The energy releases from the redox reaction is thus supplied to accelerate the whole combustion reaction. The TG analysis shows the maximum weight loss occurs in a very narrow temperature range, which corresponds to the decomposition step. The observed weight loss associated with this exothermic reaction is approximately 95%. Table-1 summarizes the effect of the amount of citric acid and pH of the starting solution. It is very interesting finding that at higher pH values the pure phase can be obtained in the as synthesized powder.

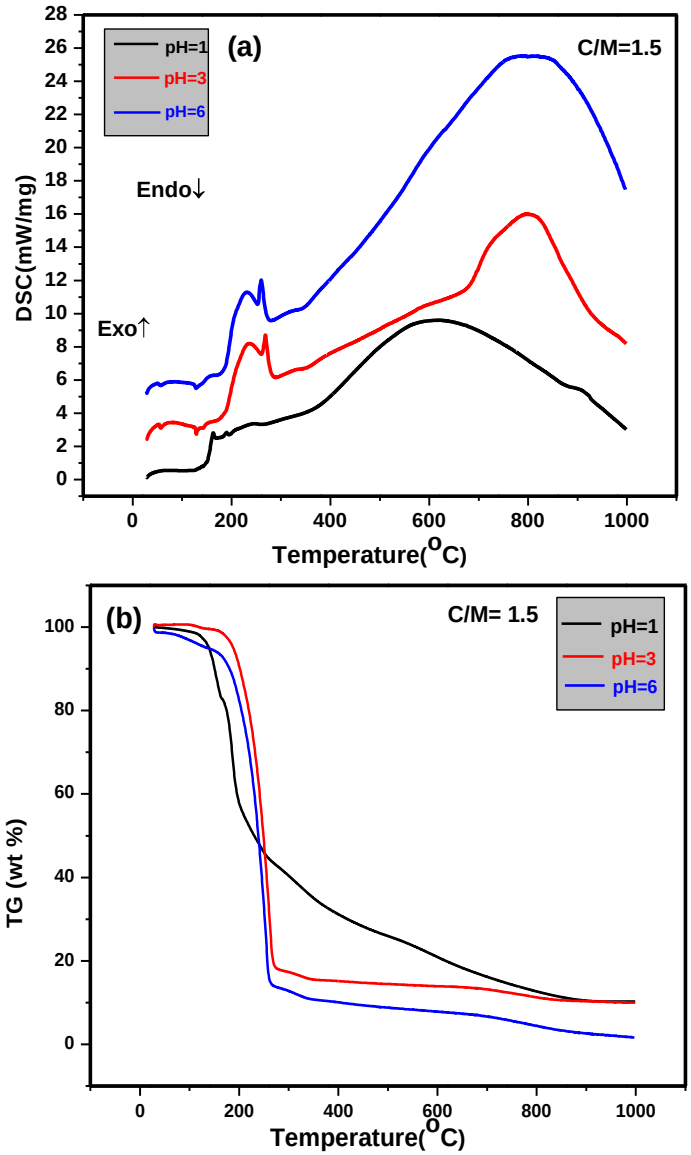

Fig. 5.9 (a) DSC and (b) TG curves of the gels for C/M=1.5 for different pH

The combustion was not so vigorous and no flame has been seen during the combustion for samples prepared at pH=1 because at this low pH value citric acid poorly dissociates and does not form a complete complex with the metal ions.

The citric acid has dual role, it acts as chelating agent for metal ions and also acts as a fuel in redox reaction. The mechanism of chelation is shown below:

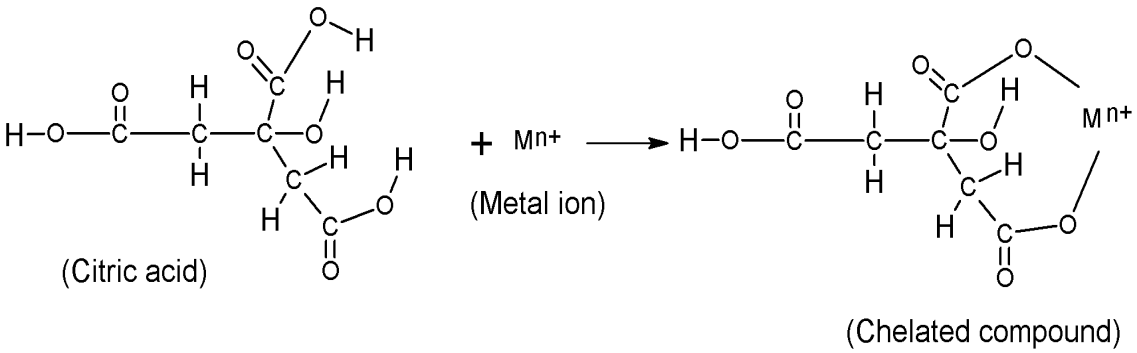

The plausible chemical reaction during the auto combustion is as follows:

$$2Li^{+}+Ti^{4+}+12NO_3^{-}+C_6H_8O_7 \rightarrow Li_2TiO_3+12NO_2+6CO_2+4H_2O$$

But for pH=3, 6 the combustion process was quite vigorous. This can be explained by the fact that additions of ammonia solution facilitate the dissociation of citric acid that is the hydrogen ions of citric acid were dislodged by OH^- ions of NH_4OH to form H_2O. Hence a better complex formation takes place. With the water evaporation the gel was formed and it start to swell, it may be due to the decomposition of citric acid ions to aconitic acid ($C_5H_6O_6$) at 175^oC and as the exothermicity of the solution increases it further yields itaconic acid ($C_5H_6O_4$ and CO_2) undergoes polymerization and swells with the de-carboxylation, releasing CO_2 [5]. Further the viscosity of the solution raised due to the crosslinking of carboxylato–metal complexes into a three dimensional network structure. As pH value increased, the network structures were developed in the gels. The gel precursors become black and a lot of pores exist in the network structures. The formation of the porous network structures may be originated from the liberation of gasses, such as NH_3, NO_x and H_2O [6]. Because the NO_3^+ ions in gel provide an in situ oxidizing environment for the decomposition of the organic component, as well as the heat released from the exothermic reaction, the rate of oxidation reaction relatively increases,

resulting in a self-propagating combustion process. The porous network structures make the materials burn rapidly and violently with burning flame. Further the NH_4^+ ions combine with the free NO_3^- ions of Ti-nitrate solution to form NH_4NO_3 which acts as an oxidizing agent and provide the heat for the reaction during exothermic redox reaction involving ammonium nitrate–citrate anions. It was found to be sufficient for the complete calcination of the compounds and water removal [7]. NH_4NO_3 may decompose to liberate NOx and O_2 following the reaction formula:

$$NH_4NO_3 \rightarrow NO_x + O_2 + H_2O$$

The oxygen can accelerate the combustion process and a great amount of heat generates in this exothermic reaction. This results in violent combustion with burning flame.

5.8 Sintering characteristics and Microstructure:

Keeping in mind the surface area, crystallite size and particle size of the Li_2TiO_3 sample we have chosen LT2 and pH3LT3 samples, for sintering and other characterization. Fig. 5.10 exhibited the percentage of thermal shrinkage [$(dL/L_0) * 100$] versus temperature, where L_0 is the initial length. For the solid state synthesized powder (10.5 m^2/gm), shrinkage onset commences in the region of 900^{o}C whilst the overall linear shrinkage is approximately 12% 1100^{o}C. For the pH3LT3 (34 m^2/gm) powder, the rate of shrinkage is sharper with a final linear shrinkage of approximately 16%. For the LT2 (62.5 m^2/gm) powder sample, shrinkage commences at lower temperatures 650^{o}C with a final linear shrinkage of approximately 16.5% by 1050^{o}C. LT2 sample has a smaller crystallite size and high surface area which helps the acceleration of sintering at low temperature.

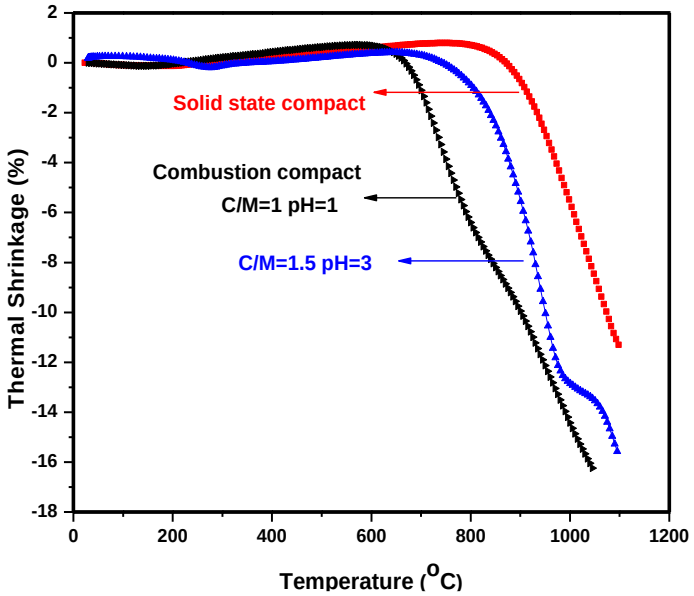

Fig. 5.10 Shrinkage behavior of different Li_2TiO_3 compact

The shrinkage rate of the powder of combustion process reached the peak value at about 737°C, 882°C for LT2 and pH3LT3 respectively. These values are nearly 200°C and 50°C lower than that of the powder obtained by sol-gel technique [8], indicating higher sinterability of the powder obtained by solution combustion method.

Fig.5.11 depicts the effect of sintering temperature on the sintered density for the different samples. The relative density of sintered LT2 compacts at 900°C for 6hr has been found to be more than 90% of theoretical density. But at same temperature pH3LT3 compacts gives 88% of theoretical density. Whereas for solid state sintered sample only 75% density can be achieved. The possible reason may be the lowering in surface area and crystallite size of combustion synthesized powder relative to solid state prepared powder.

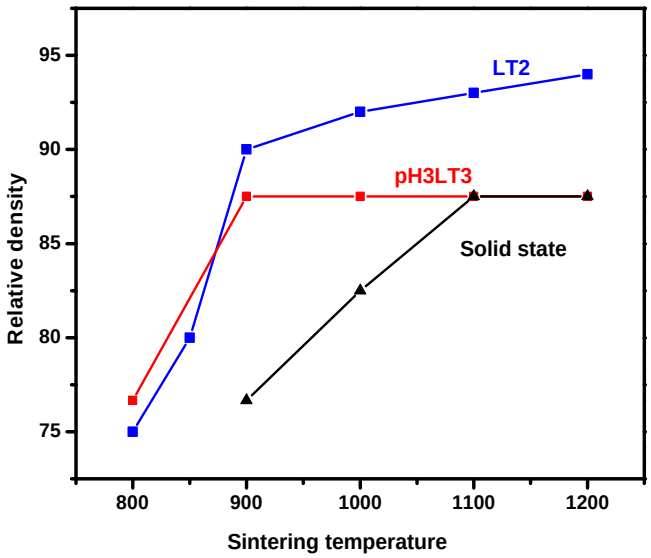

Fig. 5.11 Relative Density of Li_2TiO_3 pellets synthesized by various processes

In order to see the densification behavior at high temperature all samples were heat treated at 1000^{o}C/4hrs and 1100^{o}C/2hrs. The idea behind reducing the soaking period is to minimize the grain growth in final stage of sintering. It is evident from the figure that the density of LT2 sample increases with increase in sintering temperature that is due to the formation of liquid phase. Fig. 5.12 a&b shows the microstructure of as fired sample and fractured surface respectively of LT2 sample fired at temperature 900^{o}C. Both the sample shows dense microstructure which is corroborating our density result.

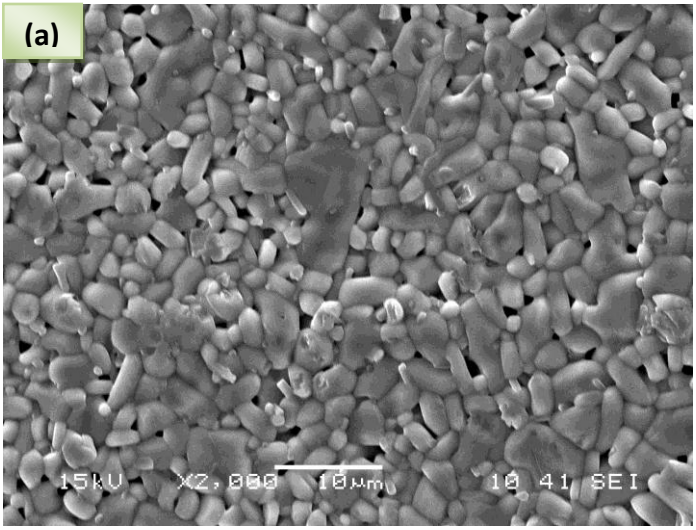

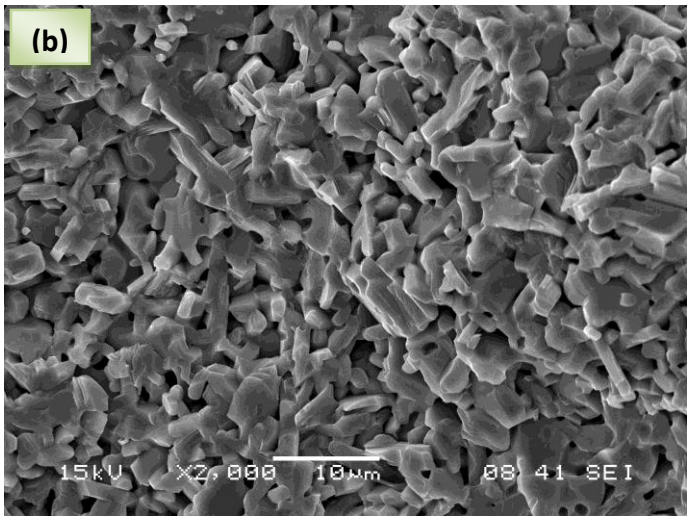

Fig. 5.12 SEM micrograph of LT2 sintered at 900^{o}C (a) as fired surface (b) fracture surface

It is interesting to mention that grain size and morphology in the sintered product strongly depends on the powder synthesis technique and sintering temperature. LT2 sample sintered at 900^{o}C shows elongated grain with a size in the range of 4-6 µm but at 1100^{o}C sintered sample shows (Fig.5.13 (a),(b) large irregular shaped fused grain (20-40 µm). Fractured surface of 1100^{o}C sintered sample shows (Fig.5.15 (a),(b) significant amount of closed pore whereas it is absent in 900^{o}C sample and that may be due to high grain growth rate and formation of liquid phase at high temperature.

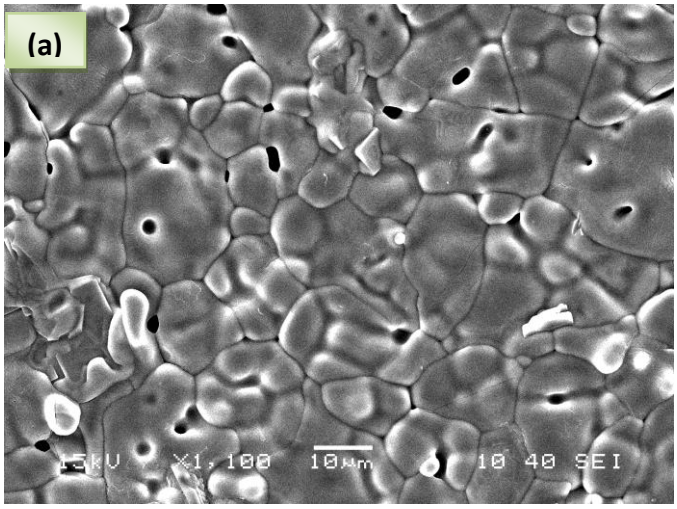

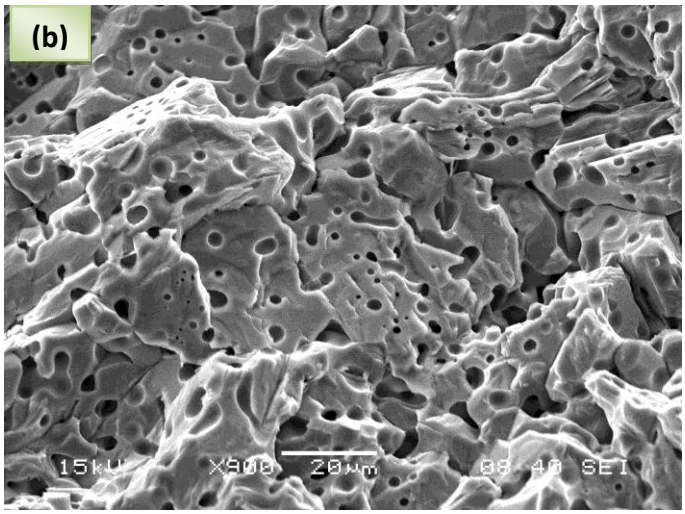

Fig. 5.13 SEM micrograph of LT2 sintered at 1100^{o}C (a) as fired surface (b) fracture surface

Whereas, pH3LT3 sample sintered at 900^{o}C shows (Fig. 5.14 (a),(b) almost round shape grain with a size in the range of 1-4 µm and contains more porosity. Fig. 5.16 (a),(b) shows that powder prepared by solid state route when sintered at 1100^{o}C depicts inhomogeneous distribution of grain size (5-30 µm) with significant amount of closed pore entrapped inside the grain as found from the fractured surface.

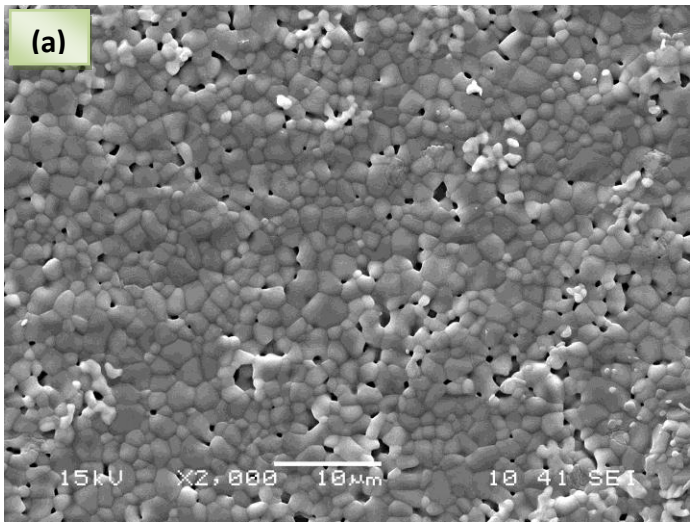

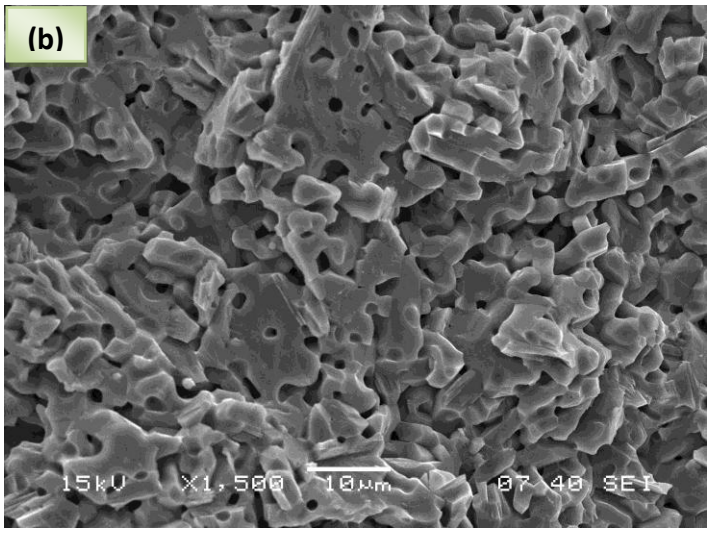

Fig. 5.14 SEM micrograph of pH3LT3 sintered at 900^{o}C (a) as fired surface (b) fracture surface

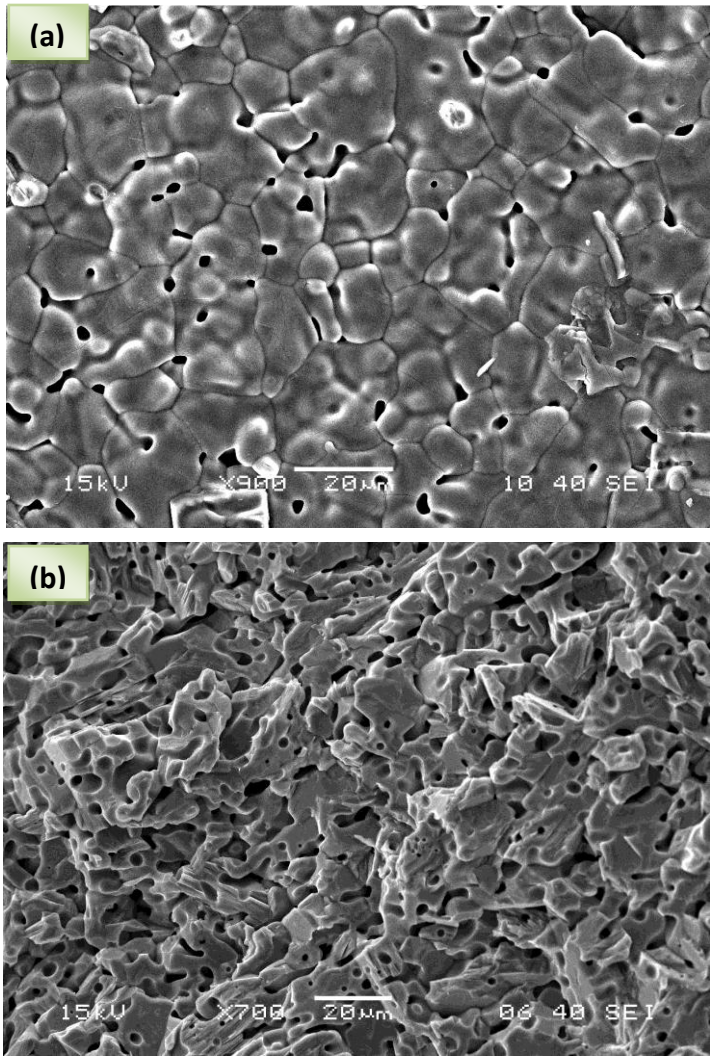

Fig. 5.15 SEM micrograph of pH3LT3 sintered at 1100^{o}C (a) as fired surface (b) fracture surface

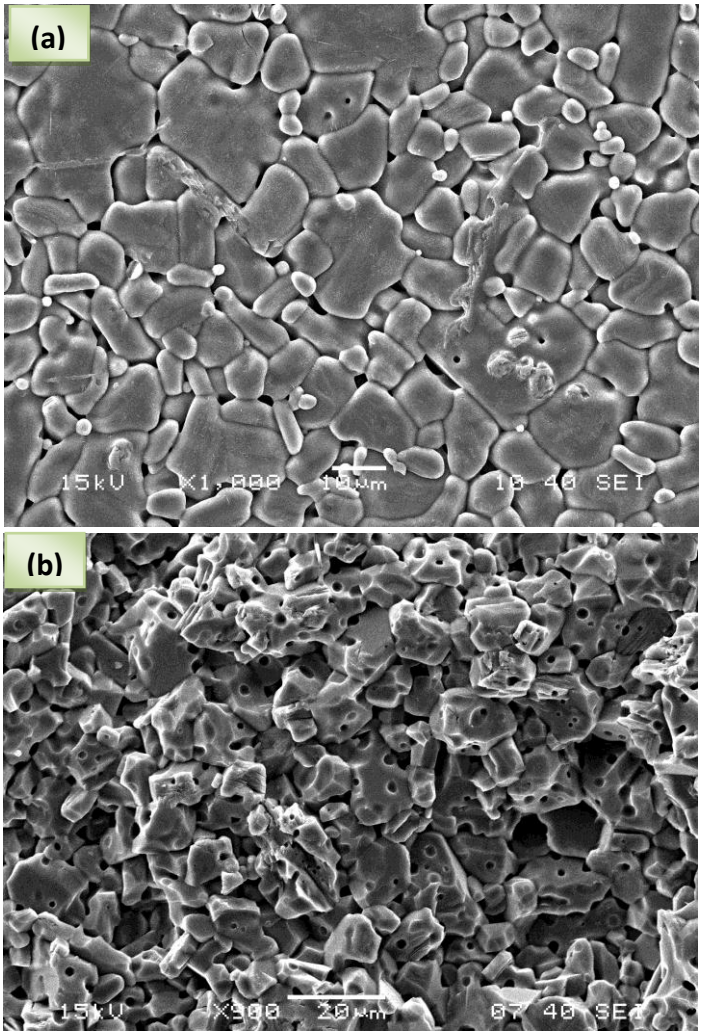

Fig. 5.16 SEM micrograph of Li_2TiO_3 prepared by solid state route, sintered at 1100^oC
(a) As fired surface (b) Fracture surface

As found from several literatures [9, 10], the densification of Li_2TiO_3 is quite difficult because of its fast grain growth at relatively higher sintering temperature. A rapid grain growth results in several large pore traps in over-sized grains or on grain boundaries. These closed pores were difficult to remove during any additional sintering process. The large grain size is deleterious regarding tritium release since the tritium ion has to follow a large path in order to come out of the breeder grain. Generally large diffusion path of tritium ion results in entrapment of the said ions in the grain. Hence small grain size is required since it reduces the diffusion path and ensures release of more number of tritium. So it can be concluded that in order to avoid the fast grain growth the sintering temperature should have to be kept low and to get significant densfication combustion synthesized powder has to be used.

5.9 Thermal expansion behavior of sintered specimen:

The thermal expansion behavior was investigated by thermo dilatometery of sintered specimens in air atmosphere. This is very important characteristics because expansion at the working temperature often results in crack generation in the material which results in the fragmentation and finally collapse of the specimen. During operation, thermal stress arises from the temperature distribution in the blanket and difference in thermal expansions between the bed and structural materials. The thermal expansion is the origin of thermal stress and is an important aspect of the thermo-mechanical analysis.

The percent change in thermal expansion (%ΔL/Lo) for the different temperature sintered sample was found to be same (0.9%). However the expansion coefficient values differ a bit for LT2 and pH3LT3. The expansion coefficient for LT2 sintered at 900^{o}C is 19.26*10-6 K^{-1} and that for pH3LT3 is 18.86×10^{-6} K^{-1}. The obtained values are in good agreement with the literature values, required during the optimal operating condition [11, 12].

5.10 Electrical conductivity:

AC impedance methods are widely used to characterize electrical materials [13]. Complex impedance formalism is commonly employed to understand electrical response of polycrystalline materials. Fig. 5.17(a) & (b) shows complex plane impedance plots of the sample LT2 and pH3LT3 respectively for three temperatures (measured impedance data were converted to specific data taking into account the geometrical shape of the sample). At lower temperature (<200^{o}C) high impedance of the sample indicates the insulating behavior. As the temperature increases above 280^{o}C fully developed semicircle is started to form. At 300^{o}C, a slightly depressed semicircular arc is seen next to the coordinate origin. At a higher temperature of 500^{o}C, a second very small arc comes into play in the low frequency region. The data points of the 300^{o}C and other temperature arc were fitted using the CNLS fitting routine LEVMW [14]. A simple equivalent circuit, describing symmetric depressed semicircular arcs, is given by the so called distributed element ZARC (Cole–Cole response) which consists of a resistance R in parallel to a CPE element. The CPE impedance is given by $Z(\omega)=A^{-1}\,(i\omega)^{-\alpha}$, ω is the angular frequency, A and α are real constants and $i=(-1)^{0.5}$ [15]. The range of α is $0\leq\alpha\leq1$; the CPE acts like a capacitor with some kind of capacitance. For α=1, an ideal semicircle occurs with the center on the Z′ axis and the mentioned circuit is given by a

resistance R in parallel to a capacitance C. From the maximum of the arcs, the approximate capacitance related to the arcs is C~15–20 pF/cm which is within the range expected for the bulk of Li_2TiO_3. The semicircle at higher frequency side indicates effect of grain conduction and at low frequency side at high temperature reflects either the effect of grain boundary or due to electrode effect. If Li^+ ions are the only charge carriers, semicircle in the high-frequency region can be concluded due to the bulk material [16].

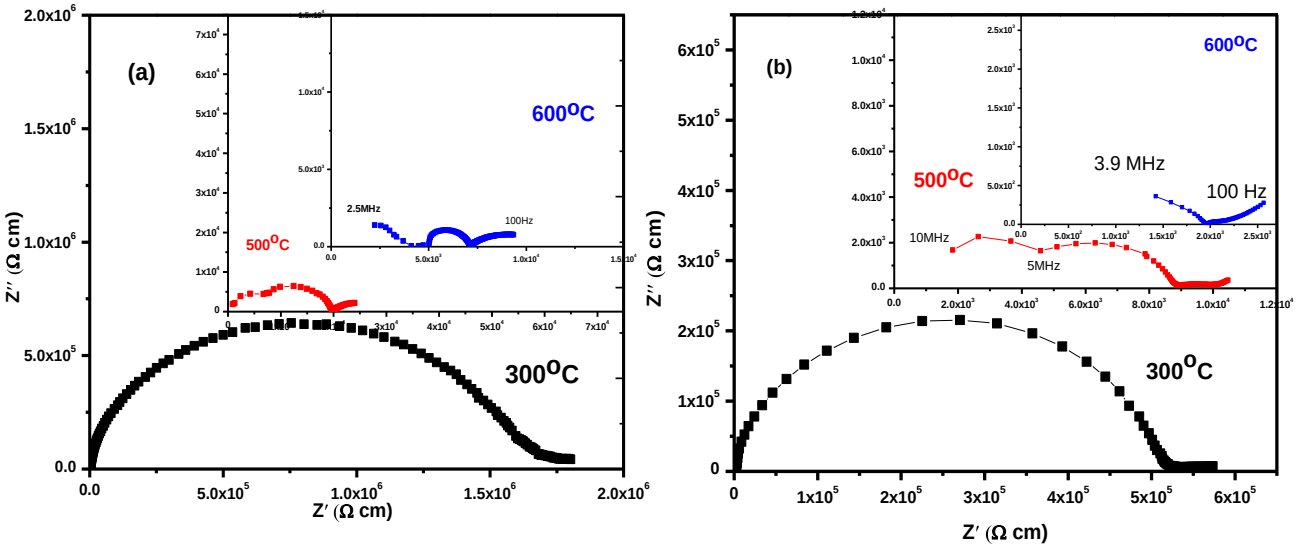

Fig. 5.17 Cole Cole plot at different temperature (a) LT2 (b) pH3LT3 (Sintered at 900°C)

Fig. 5.17(b) shows different semicircular arcs for pH3LT3. Around 500°C temperature, the onset of a further low frequency spike can be recognized along two semi circle.

In Fig. 5.18(a), (b) shows the dependence of conductivity on temperatures of LT2 and pH3LT3 (sintered at 900°C) for different frequencies along with data of σ_{dc}. At lower temperatures, the high frequency $\sigma_{ac}(\omega)$ is considerably enhanced relative to low frequency conductivity and dc conductivity. This is expected because dc conductivity is determined by the most difficult transition in complete percolation paths between the electrodes, while ac conductivity is determined by the easiest local movement of the charges. Also, $\sigma_{ac}(\omega)$ increases with rise in temperature which signifies that the electrical conduction in the material is a thermally activated process. At higher temperatures dc and ac conductivity values become closer that may be attributed to intrinsic conductivity of the materials in this temperature range [17]. There is a discontinuous change in slope of log σ_{dc} or σ_{ac} −1/T plot around ~500-600°C. This break in slope corresponds to different activation energy in two different temperature regions. It may be

attributed to a first-order phase transition. However, no previous DSC or DTA study of Li_2TiO_3 confirms any structural transition [18-20]. It is likely that transition is just displacive or disordering type with only a slight increase in the entropy and has very little change on the thermal capacity of the material [21]. Roux et.al. [18] reported changes in the x-ray diffraction pattern. However, no clear explanation is provided on this effect. However further studies are required to understand the behavior. However, from the conductivity plot it is seen that the conductivity dependence of temperature for the materials studied cannot be described by a single straight line which obeys the equation $\sigma T = \sigma_o \exp(-Ea/KT)$. For LT2 sample, three different slopes can be found out for three different temperature regions. The activation energies of LT2 Ea= 0.64 eV in the high, 0.367eV in the medium and 0.25 eV in the low temperature ranges. Whereas, for pH3LT3 sample activation energies are Ea= 0.91 eV in the high, 0.33eV in the medium and 0.28 eV in the low temperature ranges. The magnitude of such E_a values is compatible with ionic Li^+ hopping processes.

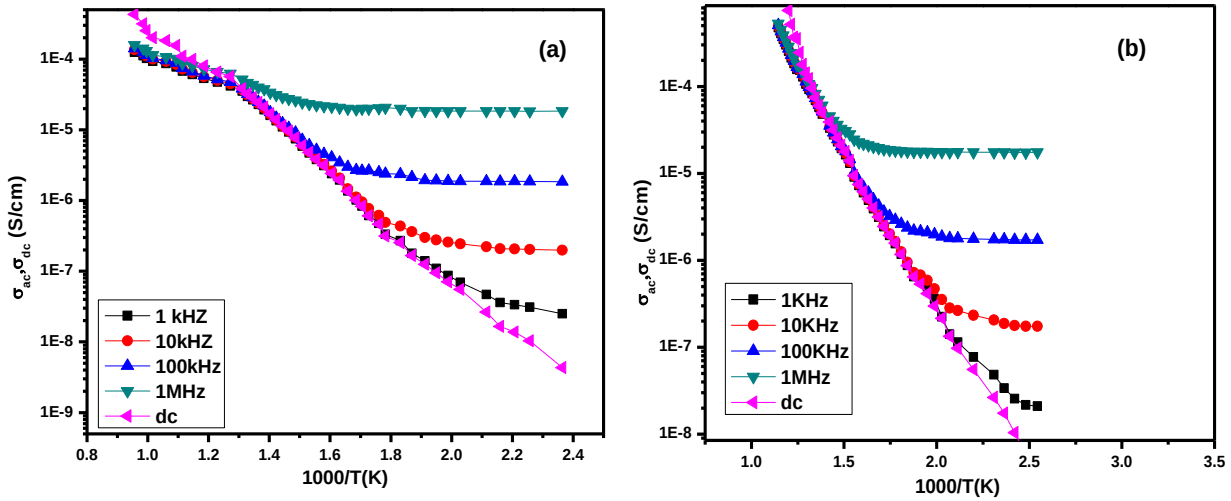

Fig. 5.18 Temperature dependence of ac and dc conductivity (a) LT2 (b) pH3LT3 (Sintered at 900^{o}C)

Fig. 5.19 (a), (b) shows the dependence of conductivity on temperatures of LT2 and pH3LT3 (sintered at 1100^{o}C) for different frequencies along with data of σ_{dc}. It is clear from the graph that LT2 sample has slightly higher conductivity compared to pH3LT3. Another interesting feature is that discontinuous change in slope in the range of 500-600^{o}C is not prominent for both the sample. The higher conductivity of LT2 sample can be explained by considering the grain size of the two samples. LT2 sample has higher grain size as depicted from the

microstructure. It is well known that ion conduction paths within a crystal are often impeded at a grain boundary due to the lattice mismatch [22].

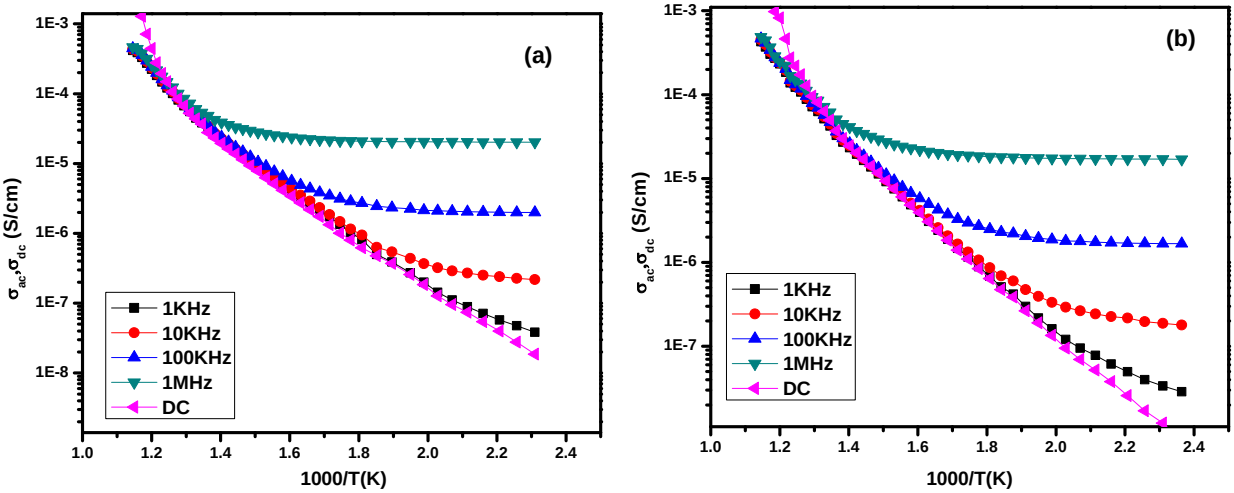

Fig.5.19 Temperature dependence of ac and dc conductivity (a) LT2 (b) pH3LT3 (Sintered at 1100^{o}C)

5.11 Thermal conductivity:

Fig. 5.20 shows the thermal diffusivity plot for LT2 and pH3LT3 samples sintered at 900^{o}C. The diffusivity for LT2 is more as compared to pH3LT3; it may be due to the difference in density between the samples. The diffusivity at lower temperature is higher and decreased as the temperature is increased. From the diffusivity data thermal conductivity has been calculated from the formula $k=\alpha C_p \rho$, where k is thermal conductivity in W/m/K, and ρ is the density in gm/m^3 α is diffusivity. The thermal conductivity has been calculated to be 2.5 W/m/K at 800^{o}C.

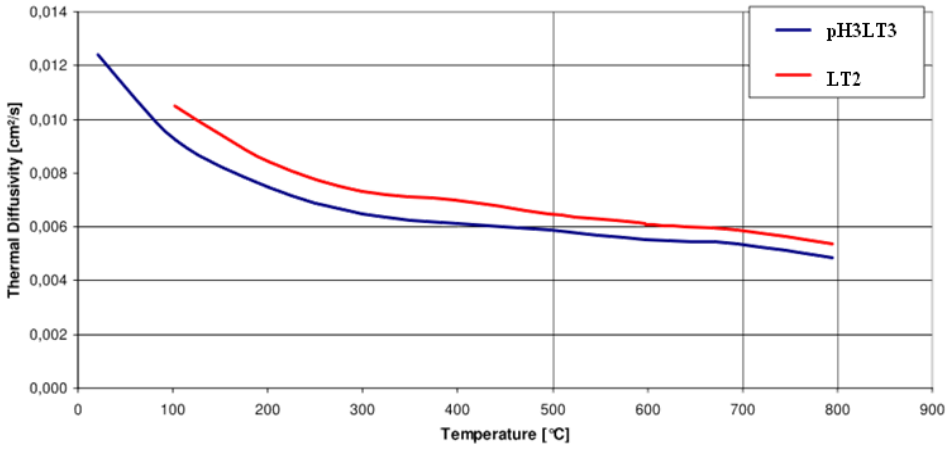

Fig. 5.20 Temperature dependence of thermal diffusivity

5.12 Neutron activation studies of powder:

The impurity content in the breeder material should not absorb neutrons and give any long lived activation product. So it is necessary to study these two aspects by irradiating the material by 14 Mev neutrons. The measured γ- peaks from the irradiated sample shows the presence of titanium, iron and potassium in Li_2TiO_3 powder. The γ-ray energies and counts recorded in the γ-spectrum are tabulated in (Table 5.3).Surprisingly, aluminium which is reported 0.3wt% in the elemental composition is not recorded in the γ-ray spectra during the first test (Fig. 5.21).

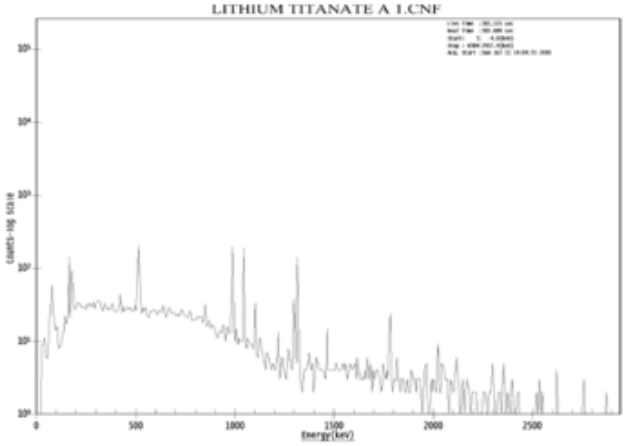

Fig. 5.21 1st test γ-spectrum of Li_2TiO_3 powder

Table 5.3 Measured γ-peaks from irradiated Li_2TiO_3 powder:

S. No.	γ–Energy (keV)	Counts (error)	Counts/sec	Pathway
1	159.1	460 +/- 5.42%	1.53	$^{47}Ti(n,p)^{47}Sc$
2	175	240 +/- 8.73%	0.80	$^{48}Ti(n,p)^{48}Sc$
3	511	1053 +/- 3.88%	3.49	β^+ annihilation
4	847.1	35 +/-37.8%	0.12	$^{56}Fe(n,p)^{56}Mn$
5	983.8	997 +/- 3.35%	3.31	$^{48}Ti(n,p)^{48}Sc$
6	1037.7	944 +/- 3.52%	3.13	$^{48}Ti(n,p)^{48}Sc$
7	1097.6	88 +/- 15.37%	0.29	?
8	1293.9	147 +/- 9.94%	0.49	$^{41}K(n,p)^{41}Ar$
9	1312.3	783 +/- 3.65%	2.60	$^{48}Ti(n,p)^{48}Sc$
10	1461.2	60 +/- 15.7 %	0.20	^{40}K(naturally occurring in lime)
11	1779.3	141 +/- 9.12%	0.47	$^{48}Ti(n,p)^{48}Sc$

So the samples were again irradiated for 3 minutes because aluminium gives short lived activity. The gamma spectrum for 3 min irradiation is shown in (Fig. 5.22).

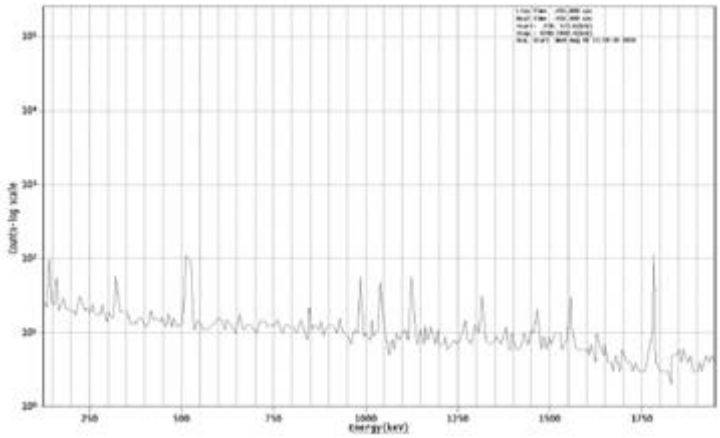

Fig. 5.22 2nd test γ-spectrum of Li_2TiO_3 powder confirming the presence of aluminum

Table 5.4 Measured γ-peaks from irradiated Li_2TiO_3:

S. No.	γ–Energy (keV)	Peak Counts	Counts/sec	Pathway
1	139.71	228	0.53	?
2	159.51	220	0.51	$^{47}Ti(n,p)^{47}Sc$
3	320.77	248	0.57	$^{50}Ti(n,g)^{51}Ti$
4	525.12	350	0.81	$^{50}Ti(n,p)^{50}Sc$
5	846.32	68.3	0.16	$^{27}Al(n,p)^{27}Mg$
6	986	262	0.61	$^{48}Ti(n,p)^{48}Sc$
7	1040.25	263	0.61	$^{48}Ti(n,p)^{48}Sc$
8	1123.97	228	0.53	$^{50}Ti(n,p)^{50}Sc$
9	1297.54	16.4	0.04	$^{48}Ti(n,p)^{48}Sc$
10	1557.17	218	0.51	$^{50}Ti(n,p)^{50}Sc$
11	1783.21	926	2.14	$^{27}Al(n,g)^{28}Al$ $^{28}Si(n,p)^{28}Al$

The counts rates and path way of measured nuclides are shown in Table 5.4 .The tritium activity in the irradiated samples is low which can't be measured by the liquid scintillaton detector. Further studies are required to understand tritium activity of irradiated Li_2TiO_3 samples.

References:

1. Kleykamp H., Fusion Eng. Des. 61-62, (2002), 361-366.
2. Yue Z., Guo W., Zhou J., Gui Z., Li L., J. Magm. Magn. Mater. 270, (2004), 216–223.
3. Gea L., Zhoua W., Rana R., Shao Z., Liu S., J. Alloys Compd., 450, (2008),338–347.
4. Guo R. S., Wei Q. T., Li H. L. and Wang F. H., Mater. Lett., 60, (2006), 261–265.
5. Pathak L.C., Singh T.B., Das S., Verma A.K., Ramachandrarao P., Mater. Lett. 57, (2002), 380–385.
6. Cannas C., Falqui A., Musinu A., Peddis D.and Piccaluga G., J. Nanoparticle Res., 8, (2006), 255–267.
7. Aruna S. T., Mukasya A. S., Current Opinion in Solid State and Materials Science, 12, (2008), 44–50.
8. Wu X., Wen Z., Lin B., Xu X., Mater. Lett., 62, (2008), 837– 839.
9. Jung C.H., Lee S.J., Kriven W.M., Park J.Y., Ryu W.S., J. Nucl. Mater., 373(2008), 194-198.
10. Rhee Y.W., Yang J.H., Kim K.S., Kang K.W., Song K.W.,Kim D. J., Thermochimica Acta, 455, (2007), 86–89.
11. Tanigawa H., Enoeda M., Akiba M., Fusion Eng. Des., 82, (2007), 2259–2263.
12. Gierszewski P., Fusion Eng. Des., 39–40, (1998), 739–743.
13. Macdonald J.R. (Ed.), Impedance Spectroscopy Emphasizing Solid Materials and Systems, John Wiley, New York, 1987, pp. 2–6.
14. Macdonald J.R., Solid State Ionics 25–28, (2005), 1961.
15. Macdonald J.R. (Ed.), Impedance Spectroscopy Emphasizing Solid Materials and Systems, John Wiley, New York, 1987, pp. 346.
16. Fehr Th., Schmidbauer E., Solid State Ionics, 178, (2007), 35–41.
17. Rao K.S., Prasad D.M., Krishna P.M., Tilak B., Varadarajulu K.C., Mater. Sci. Eng., B 133, (2006), 141.
18. Roux N., JAERI Conference (98-006) Mito, Japan, (1997), pp. 139-147.
19. Mikkelsen J.C., J. Am. Ceram. Soc., 63, (1990), 331.
20. Castelanos M., West A.R., J Mater. Sci., 14, (1979), 450.
21. Vitins G., Kizane G., Lusis A., Tiliks J., J. Solid State Electrochem. 6, (2002),311.
22. Hench L.L., West J.K., Priciples of Electronic Ceramics John Wiley & Sons, Singapore (1990), pp163.

Chapter VI

Conclusions and Scope for Future Work

6.1 Conclusions:

The research work embodied in this dissertation can be divided into three parts. The first part deals with the synthesis of phase-pure Li_2TiO_3 powder and its characterization. The second part deals with the densification study and microstructure of different route prepared powder. Third part deals with the studies of electrical conductivity, thermal expansion and thermal conductivity on the sintered sample and neutron irradiation behavior on combustion synthesized powder.

1. (a) We have synthesized Li_2TiO_3 powder by solution combustion technique using alternative precursor of titanium i.e. TiO_2. In our work Ti-nitrate solution was made stable by preparing via sulfate route. Using the stable Ti-nitrate solution and citric acid as a fuel/complexing agent in controlled amount, nanoparticles of Li_2TiO_3 have been synthesized successfully by citrate-nitrate auto-combustion route.

(b) We found that by controlling the citrate to metal ratio, phase pure powder can be found at 600^oC for C/M ratio 1 and 1.5. We observed that lower C/M ratio generates precipitation at the time of gelation and that is primarily due to poor chelation of all metal ions by citric acid. It was found that by varying pH (pH value 1, 3 and 6) of the starting solution (by adding ammonia) the phase formation takes place during the auto-combustion stage itself (for pH value 3 and 6). The phase formation at combustion stage is attributed to the higher ignition temperature and exothermicity of combustion reaction.

(c) The particle size of Li_2TiO_3 powder (prepared at C/M=1 and pH=1) was found to be 100-200 nm and surface area was 62 m^2/g. For higher pH value the surface area decrease sharply in the range of 25-40 m^2/g. This contrasts with surface area of 10.55 m^2/g of solid state mixing prepared powder. Hence, the first route is preferable to the second route (solid state route). Inductively Coupled Plasma Atomic Emission Spectrometry study shows that 0.3 wt% Al present in the Li_2TiO_3 powder.

2. It has been found that Li_2TiO_3 powder can be sintered at a temperature as low as 900^oC with a density more than 90% of the theoretical density. Li_2TiO_3 powder prepared by solid state route required higher sintering temperature (more than 1100^oC) to get more than 85% density and that produces exaggerated grain growth with a huge amount of

closed porosity. It is seen that for combustion synthesiszed powder on depending on the sintering temperature grain size may vary from 2-50 μm.

3. (a) The thermal expansion behavior was investigated by thermo dilatometery of sintered specimens in air atmosphere. Thermal expansion coefficient found to be around 19 x $10^{-6}/^{o}$C. Thermal diffusivity measured by laser flash method. Thermal conductivity value depends on the density of the sample. For LT2 sample it is found to be 2.5 W/m/K.

(b) AC impedance method has been used to characterize electrical property of the sintered sample. Impedance data, measured on sample of small grained Li_2TiO_3ceramics, showed differences for different sintering temperature in air which is doubtless an effect of the variation in microstructure. A characteristic change in slope of the dc conductivity ($\sigma_{dc)}$ with temperature around 500-600^{o}C points to a changed conduction mechanism at higher temperatures that may be due to a first order phase transition and the lithium ion structure is altered.

(c) Neutron activation studies have been done on Li_2TiO_3 powder to find out whether impurity content in the breeder material absorbing the neutrons and forming any long lived activation product. Surprisingly, aluminium which is reported 0.3wt% in the elemental composition is not recorded in the γ-ray spectra during the first test. The tritium activity in the irradiated samples is low which can't be measured by the liquid scintillation detector.

6.2 Future Work:

1. Optimized process parameter in solution combustion synthesis can be used for large scale production of the Li_2TiO_3 powder by spray pyrolysis technique using spray pyrolyser.
2. Details structural and electrical conductivity study to find out anomaly in the conductivity plot at higher temperature.
3. Pebble formation by extruder spherodizer.

.

.

Publications resulting from the M. Tech (Res) work

1. **Bhabani Sankar Sahu**, S. Bhattacharyya, P.Chaudhuri, R.Mazumder "Effect of pH and metal to citrate ratio on the synthesis and sintering of auto combustion derived Li_2TiO_3". (Communicated)
2. **Bhabani Sankar Sahu**, S. Bhattacharyya, P.Chaudhuri, R.Mazumder"Synthesis and sintering of nanosize Li_2TiO_3 ceramic breeder powder prepared by auto combustion technique" Proceedings of 20th Annual Conference of Indian Nuclear Society (INSAC-2009),(January 4-6, 2010), Chennai, India

Conferences:

1. **Bhabani Sankar Sahu**, S. Bhattacharyya, P.Chaudhuri, R.Mazumder "Synthesis of nanosize Li_2TiO_3 ceramic breeder powder by autocombustion technique" Annual General Meeting of MRSI 2010, Sardar Patel University, Vallabh Vidya Nagar, Ahmedabad.

2. **Bhabani Sankar Sahu,** Ranabrata Mazumder "Synthesis of Low Loss Lead free BNT-BT Piezoelectric Ceramics by Auto Combustion Technique" International Conference on Active/Smart Materials (January 7-9, 2009), Thiagarajar College of Engineering, Madurai, INDIA

Curriculum Vitae

Bhabni Sankar Sahu
S/O Mr. K.C. Sahu
G/45, New LIC Colony
Civil Township, Rourkela-769012,
District- Sundergarh, Orissa, INDIA.
Phone No: +91-9853178954 (M)
Email:bhabani.abc@gmail.com

Date of Birth: 17.02.1985

Education: M.Sc. (Physics)

Publications:

1. **Bhabani Sankar Sahu**, S. Bhattacharyya, P.Chaudhuri, R.Mazumder "Effect of pH and metal to citrate ratio on the synthesis and sintering of auto combustion derived Li_2TiO_3". (Communicated)
2. **Bhabani Sankar Sahu**, S. Bhattacharyya, P.Chaudhuri, R.Mazumder"Synthesis and sintering of nanosize Li_2TiO_3 ceramic breeder powder prepared by auto combustion technique" Proceedings of 20th Annual Conference of Indian Nuclear Society (INSAC-2009),(January 4-6, 2010), Chennai, India

Conferences:

1. **Bhabani Sankar Sahu**, S. Bhattacharyya, P.Chaudhuri, R.Mazumder "Synthesis of nanosize Li_2TiO_3 ceramic breeder powder by autocombustion technique" Annual General Meeting of MRSI 2010, Sardar Patel University, Vallabh Vidya Nagar, Ahmedabad.
2. **Bhabani Sankar Sahu,** Ranabrata Mazumder "Synthesis of Low Loss Lead free BNT-BT Piezoelectric Ceramics by Auto Combustion Technique" International Conference on Active/Smart Materials (January 7-9, 2009), Thiagarajar College of Engineering, Madurai, INDIA